Cytokine 118 (2019) 144–159

Contents lists available at ScienceDirect

Cytokine

journal homepage: www.elsevier.com/locate/cytokine

Novel 1,3,4-thiadiazoles inhibit colorectal cancer via blockade of IL-6/COX-2 mediated JAK2/STAT3 signals as evidenced through data-based mathematical modeling

Vinit Raj[a], Archana S. Bhadauria[b], Ashok K. Singh[a], Umesh Kumar[c], Amit Rai[a], Amit K. Keshari[a], Pranesh Kumar[a], Dinesh Kumar[c], Biswanath Maity[c], Sneha Nath[d], Anand Prakash[d], Kausar M. Ansari[e], Jawahar L. Jat[f], Sudipta Saha[a,*]

[a] Department of Pharmaceutical Sciences, Babasaheb Bhimrao Ambedkar University, Vidya Vihar, Raibareli Road, Lucknow 226025, India
[b] Faculty of Mathematical and Statistical Sciences, Shri Ramswaroop Memorial University, Deva Road, Lucknow 225003, India
[c] Centre of Biomedical Research, SGPGIMS Campus, Raebareli Road, Lucknow 226014, Uttar Pradesh, India
[d] Department of Biotechnology, Babasaheb Bhimrao Ambedkar University, Vidya Vihar, Raibareli Road, Lucknow 226025, India
[e] Environmental Carcinogenesis, CSIR-Indian Institute of Toxicology Research, Vishvigyan Bhavan, 31, Mahatma Gandhi Marg, Lucknow 226001, India
[f] Department of Applied Chemistry, Babasaheb Bhimrao Ambedkar University, Vidya Vihar, Raibareli Road, Lucknow 226025, India

ARTICLE INFO

Keywords:
1,3,4-Thiadiazole derivatives
Colorectal cancer
IL-6/COX-2 mediated JAK2/STAT3
Mathematical modeling
^{1}H NMR-based metabolomics

ABSTRACT

We attempted a preclinical study using DMH-induced CRC rat model to evaluate the antitumor potential of our recently synthesized 1,3,4-thiadiazoles. The molecular insights were confirmed through ELISA, qRT-PCR and western blot analyses. The CRC condition was produced in response to COX-2 and IL-6 induced activation of JAK2/STAT3 which, in turn, was due to the enhanced phosphorylation of JAK2 and STAT3. The treatment with 1,3,4-thiadiazole derivatives (VR24 and VR27) caused the significant blockade of this signaling pathway. The behavior of STAT3 populations in response to IL-6 and COX-2 stimulations was further confirmed through data-based mathematical modeling using the quantitative western blot data. Finally, VR24 and VR27 restored the perturbed metabolites associated to DMH-induced CRC as evidenced through ^{1}H NMR based serum metabolomics. The tumor protecting ability of VR24 and VR27 was found comparable or to some degree better than the marketed chemotherapeutics, 5-flurouracil.

1. Introduction

Colorectal cancer (CRC) is one of the most lethal cancer and causes high incidence of mortality worldwide [1]. According to American Cancer Society of the United States, about 6,00,000 cancer-related deaths and 1.7 million new cases occurred in 2015 [2]. While vast promising advancement has been accomplished for the diagnosis and treatment of colorectal cancer (CRC), it remains a foremost public health problem. There are several inflammatory targets including cyclooxygenase 2 (COX-2), interleukins (ILs) and associated intracellular signaling molecules responsible for CRC development [3–5]. 1,3,4-Thiadiazole ring has been incorporated into numerous diuretic and anticancer drugs, including acetazolamide, methazolamide and megazol. The pharmacological responses of these drugs are probably due to carbonic anhydrase enzyme inhibition properties [6–8]. However, the risk of associated side effects like blurred vision (acetazolamide and methazolamide) and genotoxicity (megazol) can reduce a patient's motivation to take their medications consistently [9]. In addition, 1,3,4-thiadiazoles exhibited promising *in vitro* cytotoxic effects against various cancer types including breast, lungs, colon and rectum [8].

Recent investigation suggested that 1,3,4-thiadiazoles are the inhibitors of COX-2 and ILs that can lead to deactivation of associated signaling molecules, including janus kinases (JAKs) and signal transducer and activator of transcriptions (STATs). Growing evidence suggested that the growth of CRC can be prevented through the down-regulation of both COX-2 and IL-6 expressions at CRC site [10–13]. In view of this, recently we designed and synthesized novel 1,3,4-thiadiazole derivatives and screened them for anticancer activity against HT-29 human colon cancer cell lines. Two compounds, VR24 and V27 (Fig. 1) showed their strong potential to inhibit the growth of CRC cells *in vitro*. In addition, they also inhibited both IL-6 and COX-2 enzymes *in vitro* during enzyme-linked immunosorbent assay (ELISA) [14]. Now, it was speculative whether these compounds have anti-CRC potential in

* Corresponding author.
E-mail address: sudiptapharm@gmail.com (S. Saha).

https://doi.org/10.1016/j.cyto.2018.03.026
Received 8 February 2018; Received in revised form 19 March 2018; Accepted 19 March 2018
Available online 23 March 2018
1043-4666/

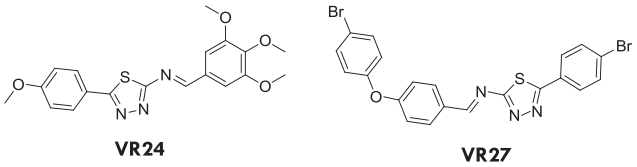

Fig. 1. Chemical structures of VR24 and VR27 (1,3,4-thiadiazoles).

the experimental *in vivo* model with a similar mechanism described in our previous *in vitro* study. Prior to performing *in vivo* antiproliferative study, an acute toxicity study was conducted in albino Wistar rats to determine the safe dose of both compounds. The study revealed that no significant toxicity was produced up to a dose of 25 mg/kg. Later, the pharmacokinetic studies of both compounds demonstrated an optimal degree of oral absorption, distribution and renal clearance [15].

In this context, we performed *in vivo* experiment to evaluate the anti-CRC action of VR24 and VR27 in DMH-induced CRC rat model and to confirm the molecular mechanism underlying their action. As preliminary investigation, various physiological, enzymatic, oxidative stress parameters, and morphological studies were conducted to assure the protective effect of VR24 and VR27.

The tissue concentration of the important inflammatory mediators (IL-2, IL-6) and enzyme (COX-2) were measured using ELISA. Further, gene and protein expression studies were performed to explore the effects of these compounds on IL-6 and COX-2 mediated activation of JAK2/STAT3. In addition, a data-based mathematical modeling was applied using the data of quantitative western blot. For this purpose, the quantitative western blot data were used into a system of differential equations formulated for individual steps of the IL-6 and COX-2 induced JAK2-STAT3 signaling pathway [16,17]. Applying the fitted mathematical model, the quantitative behavior of different STAT3 populations could be determined that was not accessible to experimental measurement. In addition, proton nuclear magnetic resonance (^{1}H NMR) based serum metabolomics study was performed to discover the metabolic perturbations during CRC condition and there regulation with VR24 and VR27 treatment.

2. Materials and methods

2.1. Drugs and reagents

1,3,4-Thiadiazole derivatives, VR24 and VR27, were already synthesized by our research group [14]. Dimethylhydrazine (DMH) was purchased from MP Biomedicals, Santa Ana, California, USA. GSH and 2,4-dinitrophenylhydrazine (DNPH) was purchased from Sigma-Aldrich, Bangalore, India. All other chemicals were procured from Himedia, Mumbai, India. All the solvents and chemicals were of analytical grades with 99% purity and in-house distilled water was used throughout the experiment.

2.2. Animals

Male albino Wistar rats (aged 2–3 months, weight 90–110 g) were used in this experiment. The protocol was approved by the Institutional Animal Ethical Committee (IAEC) before the initiation of the experiment (Ref no. AEC/PHARM/1601/04/2016/R2). All methods were followed in accordance with the relevant guidelines and regulations of IAEC. Standard laboratory conditions (temperature 25 ± 5 °C and light/dark cycle of 12 h) were maintained with free access to a commercial pellet diet and water *ad libitium*. Animals were kept for one week before starting the experiment.

2.3. Acute oral toxicity study

Acute toxicity study of VR24 and VR27 was performed orally at the doses of 5, 10 and 25 mg/kg as per the OECD guidelines for the testing of chemicals [18] as shown in Supplementary material.

2.4. Experimental protocol

All animals were randomly divided into 7 groups with 8 animals in each group (n = 8). The groups were classified as follows: group 1: 0.25% CMC (2 mL/kg normal control, NC), group 2: DMH (40 mg/kg, subcutaneously, carcinogen control, CC) [19,20], group 3: DMH + 5-fluorouracil (5-FU, 10 mg/kg, intraperitoneally, positive control, PC) [21], group 4: DMH + VR24 (10 mg/kg, orally), group 5: DMH + VR24 (25 mg/kg, orally), group 6: DMH + VR27 (10 mg/kg, orally), and group 7: DMH + VR27 (25 mg/kg, orally). The procedure to induce CRC was taken from previous literatures.

After initial one week of adaptive inhabitation, all rats of group 2–7 were administrated with DMH. DMH-induced CRC was produced by 40 mg/kg subcutaneous (s.c.) injection, once a week for 4 weeks. After 28 days of DMH treatment, 5-FU, VR24 and VR27 were administrated for 15 days in their respective groups as mentioned above. After the end of dosing experiment, the blood samples were collected by retro-orbital plexus in sterile centrifuge tubes and kept at 4 °C for 30 min. The tubes were centrifuged at 5000 rpm for 10 min, the pale yellow color supernatant was collected in another sterile microcentrifuge tube and kept at −20 °C for further analysis. Animals were then sacrificed by cervical decapitation, the colons were dissected out, unwrapped along the longitudinal median axis, rinsed immediately in ice cold saline and the inner surface was examined microscopically. Finally, it was stored at −20 °C for further studies.

2.5. Determination of physiological parameters in colon tissues

The various physiological parameters were measured as preliminary examination. The body weight of rats was measured at the initial and final days of the experiment. Tumor incidence no. was counted for each colon. The length (L), width (W) and height (H) of tumor were measured using a vernier caliper with 0.1 mm graduations, and tumor volume (TV) was calculated ($TV = l \times W \times H \times \pi/6$) [22]. The pH of colonic content was measured using a pH meter. Total acidity was determined by the titration method using 0.1 N sodium hydroxide with phenolphthalein as an indicator in the similar experiment.

2.6. Determination of enzyme levels in serum

Serum aspartate aminotransferase (AST), alanine aminotransferase (ALT), lactate dehydrogenase (LDH) and alkaline phosphatase (ALP) were measured according to the commercially available kit from Transia Biomedicals Ltd., Baddi, Himachal Pradesh, India. According to the manufacturer's protocol, 100 µL of serum samples were added in 1 mL of working reagent and measured the absorbance at 340 nm on regular intervals of 1 min for 3 min [23,24]. The calculated equation was as followed: Activity of ALT or AST (U/mL) = (ΔA_{340}/min) × 1768. On the other hand, lactate dehydrogenase (LDH) and alkaline phosphatase (ALP) were determined in the serum using a commercially available kit acquired from Agappe Diagnostics Ltd., Kerala, India [22]. Activity of LDH (U/L) = (ΔA_{340}/min) × 16030.

2.7. Determination of oxidative stress parameters

Oxidative stress parameters such as malonaldehyde (MDA) [thiobarbituric acid reactive substances (TBARS)], protein carbonyl (ProC), catalase (CAT), reduced glutathione (GSH), and superoxide dismutase (SOD) [22] levels were measured in the colon tissue. The total protein content of each sample was measured using the Bradford reagent and bovine serum albumin (BSA) was used as a standard. The detailed information on these experimental assays is provided in Supplementary materials.

2.8. Histopathology and scanning electron microscopy (SEM) analyses

Colon tissues from each group were assessed for their morphological changes using eosin and hematoxylin staining. The tissues were kept in 10% formalin overnight. Subsequently, they were superseded by 70% isopropanol overnight. Afterward, the tissues rinsed with isopropanol at various concentrations (70, 90 and 100%) and dehydrated further by 100% xylene. The tissue samples were then fixed in beeswax and 5 μM longitudinal sections were sliced using microtome. Finally, they were fixed and stained by eosin and hematoxylin dyes and examined under microscope (magnification 40 X).

For SEM analysis, 2–4 mm colon tissue samples were collected and fixed in 2.5% glutaraldehyde for 2–6 h at 4 °C for primary fixation. The samples were then cleaned with 0.1 M phosphate buffer for 15 min at 4 °C. Later, 1% osmium tetroxide was used as a post-fixation agent for 2 h at 4 °C. Again, the samples were washed in 0.1 M phosphate buffer for 3 times at 15 min interval and kept at 4 °C. The washed samples were dehydrated with acetone at various concentrations (30, 50, 70, 90, 95 and 100%). All specimens were air dried at room temperature and critical point of drying (31.5 °C at 1100 psi). Finally, tissue samples were mounted on to the aluminum stubs with adhesive tape and observed for the morphological changes using a scanning electron microscope (JEOL JSM-6490LV).

2.9. ELISA (Enzyme-Linked immunosorbent Assay)

Interleukins (IL-2: RAB0288 and IL-6: RAB0311) were measured using commercially available ELISA kit from Sigma-Aldrich, USA. COX-2 ELISA Kit (BYEK1295) was obtained from Bioseps Technology Co., LTD, China.

2.10. Quantitative Real-time polymerase chain reaction (qRT-PCR) analysis

Colorectal tissue sample (10 mg) of each group was used and total mRNA was isolated using TriaZol reagent. RNeasy mini kit was used to purify the mRNA. The concentration of mRNA present in each sample was estimated using the Nano Drop instrument at 260/280 nm. Further, complementary deoxyribose nucleic acid (cDNA) was prepared according to the manufacturer's protocol for GeneSure first strand cDNA synthesis kit (Genetix Biotech Asia Pvt. Ltd., New Delhi, India). Finally, qRT-PCR was performed in Agilent Stratagene Mx3000P series (Applied Biosystems, Foster City, USA) using Sybr® green PCR master mix. The cDNA was denatured at 94 °C for 5 min, annealed at 58 °C for 30 s and further elongation was performed at 72 °C for 35 s. Forty times repetition of the cycle was set using qRT-PCR which helps in detection of amplified DNA in real time. The mRNA was normalized with the housekeeping control β-actin. ΔCt values were normalized with the untreated control samples for all compounds ($\Delta Ct = Ct_{gene\ of\ interest} - Ct_{housekeeping\ gene}$). Relative changes in the expression level of one specific gene were calculated in terms of $2^{-\Delta\Delta Ct}$ ($\Delta\Delta Ct = \Delta Ct_{test} - \Delta Ct_{control}$) [22]. The primer sequences were as follows: IL-6, 5′-GCCCTTCAGGAACAGCTATGA-3′ (forward) 5′-TGTCAAC AACATCAGTCCC AAGA-3′ (reverse) [25]; COX-2, 5′ ATCAGAACCGC ATTGCCTCT-3′ (forward), 5′-GCCAGCAATCTGTCTGGTGA-3′ (reverse) [26]; JAK2, 5′-TTTGAAGACAGGGACCCTACACAG-3′ (Forward) 5′-TCATAGCGGCACATCTCCACA-3′ (Reverse); STAT3, 5′-TTTGAAGAC AGGGACCCTACACAG-3′ (Forward) 5′-TCATAGCGGCACATCTCC ACA-3′ (Reverse) [27]; and β-actin, 5′-AAGTCCCTCACCCTCCCAA AAG-3′ (forward) 5′- AAGCAATGCTGTCACCTTCCC-3′ (reverse) [28].

2.11. Western blot analysis

Protein expression levels of IL-6, JAK-2, p-JAK-2, STAT-3, p-STAT3 and β-actin were assessed by immunoblotting. All antibodies were purchased from Thermo Fisher Scientific, Waltham, MA, USA. Cells were lysed in radioimmunoprecipitation assay (RIPA) buffer, centrifuged at 10,000 rpm for 15 min at 4 °C and protein amounts were determined using Bradford reagent. Proteins (50 μg) were electrophoresed on 12% sodium dodecyl sulfate (SDS)-polyacrylamide gel and immediately transferred to polyvinylidene fluoride membrane. The membranes were blocked in 5% skimmed milk containing phosphate buffered saline (PBS) with 0.1% tween-20 (PBS-T) for 3 h at 4 °C and probed with primary antibodies diluted in PBS-T: IL-6, JAK-2, p-JAK-2, STAT-3, p-STAT3 and β-actin mouse monoclonal antibody (1:500 dilution of each) overnight at 4 °C. Next day, the membranes were washed with tris-buffered saline containing tween-20 (TBS-T) three times and incubated with anti-rabbit secondary antibodies linked to horse-radish peroxidase at a 1:3000 dilution at room temperature for 3 h. The film was washed three times with TBST, the membrane was developed with enhanced chemiluminescence ECL (Pierce™ ECL Western Blotting Substrate) and images were obtained using Chemidoc (Clinx Scientific Instruments, China) [29,30].

2.12. Mathematical modeling

The ordinary differential equation (ODE)-based model was used and calibrated using the MATLAB software. The dynamical parameters were taken from the previous literature [16]. The behavior of STAT3 phosphorylation was displayed by plotting the graphs of STAT3 and p-STAT3 versus time, using different values of IL-6 and COX-2 (obtained by quantitative western blot) for different studied groups. In addition, we studied the variation in behavior of STAT3, p-STAT3, dimer p-STAT3 in cytoplasm and the nuclear translocation of dimer p-STAT3 with time.

2.13. ^{1}H NMR based metabolomics spectroscopy

2.13.1. Sample preparation

All samples were thawed at room temperature, mixed well via vortex mixer and centrifuged at 10,000 rpm for 10 min to remove any excess precipitates. Serum (250 μL) were mixed with 250 μL of 0.9% saline sodium-phosphate buffer (50 mM, pH 7.4) in 100% D_2O (deuterium oxide) to minimize the variation in pH [22]. The supernatant (400 μL) was placed in 5 mm NMR tubes (Wilmad Glass, USA) for data acquisition with a co-axial insert containing 0.1% TSP (Sodium salt of 3-trimethylsilyl-(2,2,3,3-d_4)-propionic acid) as an external standard to aid metabolite quantification by ^{1}H NMR. The sodium salt TSP and D_2O were used as a co-solvent and provided a deuterium field/frequency lock. Both were purchased from Sigma-Aldrich, Rhode Island, USA.

2.13.2. ^{1}H NMR processing

NMR spectra were recorded at 298 K using Bruker Biospin Avance-III 800 MHz NMR spectrometer (equipped with Cryoprobe), set at a proton frequency of 800.21 MHz. The NMR instrument was equipped with the shielded maximum gradient-strength output of 53 G/cm. The 400 μL of serum sample was filled in 5 mm NMR sealed tube and a sealed capillary tube containing the known concentration of TSP was inserted separately for the purpose of locking and chemical shift referencing. For each serum sample, transverse relaxation-edited CPMG (Carr–Purcell–Meiboom–Gill) NMR spectra were acquired using the standard Bruker's pulse program library sequence (CPMGPR1D) with pre-saturation of the water peak by irradiating it continuously during the recycle delay (RD) of 5 s. Each spectrum consisted of the accumulation of 128 scans and lasted for approximately 15 min. A total spin–spin relaxation time of 60 ms (n = 300 and $2\tau = 200\delta$s) was applied to remove the broad signals of triglycerides, proteins, cholesterols, and phospholipids. Each free induction decay (FID) was filled to zero and Fourier-transform (FT) was adjusted to 64 K data points. All these data were analyzed using Bruker NMR data processing software Topspin-V3.0 and following manual phase and baseline was corrected through this software. A line broadening factor of 0.3 Hz and a sine–bell

apodization function was employed to FIDs before FT. After FT, the reference peak was adjusted internally to the methyl peak of lactate (δ = 1.33 ppm). The spectra were recorded using sine shaped gradient pulses of strength 30% and a duration of 1.5 ms followed by a delay of 200 μs to allow for the decay of eddy current. The relaxation delay was 4 s and water peak irradiation was applied during the recycle delay and the delay after the first Bloembergen-Purcell-Pound (BPP). A line broadening factor of 1 Hz was applied to FIDs before FT again. The FIDs were processed using exponential line broadening of 1.0 Hz; spectra were recorded with 128 scans and zero-filled to 64 K points before Fourier transformation. The raw NMR data were acquired on Topspin-V2.1 (Bruker NMR data processing software). All recorded spectra were, visually monitored for acceptability and subjected to multivariate statistical analysis to discriminate the altered metabolic patterns.

2.13.3. Spectral assignment

For the assignment of various peaks in the 1D ^{1}H-CPMG NMR spectra, chemical shifts were identified and assigned by comparing the chemical shifts using the database library of Chenomx 8.1 software NMR suite (Chenomx Inc., Edmonton, Canada). The remaining peaks in the CPMG ^{1}H NMR spectra were assigned by adopting the previously reported NMR spectra of metabolites, data obtained from HMDB (Human Metabolome Database) [31] and BMRB database (Biological Magnetic Resonance Data Bank) [32].

2.13.4. Multivariate statistical analysis

The multivariate data analysis was carried out using ^{1}H-CPMG. Before the data analysis, all the ^{1}H NMR spectra were manually phased and baseline corrected using TopSpin3.0 (Bruker NMR data Processing Software). For multivariate analysis, the CPMG (δ 8.5–0.5) ppm spectra were binned and integrated automatically using AMIX package (Version 3.8.7, Bruker, BioSpin). It is notable that the CPMG NMR is frequently used to suppress the wide peaks to assist the quantification of small molecular weight metabolites. ^{1}H-CPMG spectra have signals both from low molecular weight (MW) metabolites and lipid metabolites. The quantitative difference of lipid signals may minimize the biased significance of metabolites present in less abundant; the analysis allows better quantitative comparison of low MW metabolites and surmounts their discriminatory significance as well. Therefore, the lipid signals from the data matrix has been excluded to investigate the metabolic alterations for the metabolites other than lipids/fatty acids. Finally, the selected regions were reduced to spectral bins of (δ 0.01) ppm for CPMG spectra and each spectral bin is further normalized using the total spectral intensity to abolish the dilution effect among samples and to give the same total integration value for each spectrum.

The binned data from CPMG experiments was subjected to chemometrics data analysis using the web-based tools server MetaboAnalyst Version 3 [33,34] (http://www.metaboanalyst.ca) for statistical data modeling and analysis. The Data filtering was carried out to identify and remove variables that are unlikely to be of use when modeling the data. After the filtration of variables, interquartile range (IQR) was assigned for normalizing the each variant. After the normalization of data set, NMR variables were Pareto scaled and subsequently, subjected to unsupervised principal component analysis (PCA) for an initial overview of the grouping trend, which showed the internal structure of datasets in an unbiased way and diminishes the dimensionality of data (i.e. intrinsic clustering) and outliers within the data set. The data were further modeled with the supervised method of Partial Least Squares Discriminant Analysis (PLS-DA) to expose class separations between the groups and to identify the metabolites responsible for class separation. The validation of the PLS-DA models were measured by a permutation analysis (100 times), and the resulting cross-validation parameters R^2 and Q^2 were used to assess the quality of the PLS-DA models i.e. the goodness of prediction parameter by Q^2 (or the predictive capability of the model) and the goodness-of-fit parameter by R^2 (also referred to as explained variance). The PLS-DA model was further used to identify the metabolites responsible for the discrimination based on their higher values of variable significance on projection scores (i.e. VIPs) and showing statistical significance as estimated based on 0.05 level of probability i.e. p-value < 0.05 (calculated using Mann-Whitney test for pairwise comparisons). The VIP score represents a weighted sum of squares of the PLS loadings and acquires the amount of elucidated Y-variation in each dimension to measure the impact of each metabolite in the model. Usually, metabolites with high-impact have VIP values higher than 1. In this study, the VIP score cut-off value ≥1 for CPMG was used for discriminatory significance. Orthogonal projection to the latent structure with discriminant analysis (OPLS-DA) was employed for combined and pairwise analysis of spectral data. Next, the data were modeled with the supervised method, OPLS-DA to reveal class separations between the groups and S-plot to identify the metabolites of discriminatory relevance responsible for class separation. The cluster analysis has also been performed by using Hierarchical clusterings such as dendrogram for the measurement of similarities and average linkage into each variable.

The box plot representation and area under the curve (AUC) were measured by univariate analysis. This was related to visualizing the variation in the levels of significantly altered and discriminatory ability of metabolites as showed the potential biomarker, respectively with values close to 1 as a better classification. Moreover, T-test univariate analysis was employed to determine the significance biomarker of the variable (*p*-value) along with up and down regulation of metabolites.

2.13.5. Pathway analysis

The pathway analysis was performed using the pathways library of metaboanalyst server for mammals [*Rattus norvegicus*]. The metabolites significantly altered in the treated samples compared to the CC, which identified through PLS-DA analysis with a good VIP scores and determined the affected metabolic pathways using pathway analysis module. This is a combination of enrichment analysis and pathway topology analysis inbuilt in the MetaboAnalyst. The membrane and lipid metabolites like as LDL, VLDL, HDL, lipids, NAG, OAG were not recognized by the program; thus were excluded in this analysis. The final list of altered metabolites was uploaded and analyzed by Over-Representation analysis (ORA) in Metabo Analyst. The rat (Rattus norvegicus) pathway library, the out-degree centrality algorithms, and the hypergeometric test were employed for pathway enrichment and pathway topology analysis. The pathway analysis module provided a fit coefficient (*p*) from pathway enrichment analysis and an impact factor from pathway topology analysis for each analyzed pathway. All matched pathways are shown according to their *p*-values from the pathway enrichment analysis (vertical axis or y-axis, the intensity of color) and pathway impact values from pathway topology analysis (horizontal axis or x-axis, the size of circle), with the most impacted pathways colored in red [35,36].

2.13.6. Statistical data analysis

Statistical data analysis was carried out using the software GraphPad Prism 5.0 (San Diago, CA, USA). The results were expressed as mean ± standard deviation (SD) (n = 8). The statistical data was analyzed by one-way ANOVA (analysis of variance) followed by Bonferroni's multiple comparison test. Statistically significant differences were observed between carcinogen control (CC) and test groups [one way-ANOVA followed by Bonferroni multiple comparison test (*p < 0.1, **p < 0.01, ***p < 0.001)].

3. Results

3.1. Evaluation of physiological and biochemical parameters in colon and various enzyme levels in serum

The physiological parameters including body weight, tumor incidence number, tumor volume, pH and total acidity were measured

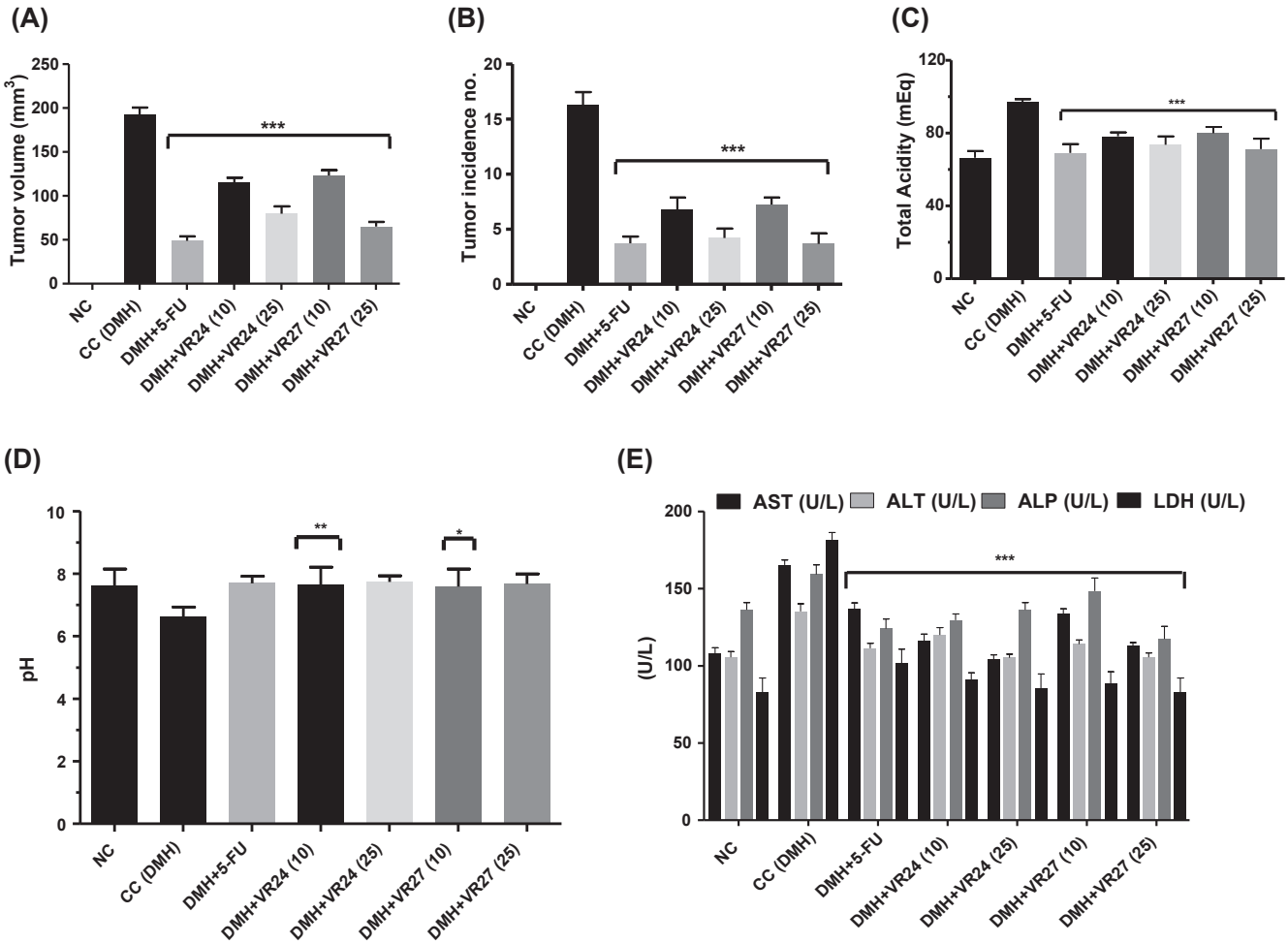

Fig. 2. Effects of VR24 and VR27 on (A) tumor incidence no., (B) tumor volume, (C) pH and (D) total acidity in colon (E) liver marker enzymes: aspartate transferase (AST), alanine transferase (ALT), alkaline phosphatase (ALP) and lactate dehydrogenase (LDH) in plasma, after 10 and 25 mg/kg doses for 15 days. Data represented as mean ± SD (n = 8). Statistically significant differences were observed between carcinogen control (CC) and test groups [one way-ANOVA followed by Bonferroni multiple comparison test (*p < 0.1, **p < 0.01, ***p < 0.001)]. NC (Normal control), DMH (Carcinogen control: CC), DMH + 5-FU (Positive control: PC), DMH + VR24(10) (Treatment A10), DMH + VR24(25) (Treatment A25), DMH + VR27(10) (Treatment B10), and DMH + VR27(25) (Treatment B25).

after oral administration of VR24 and VR27. The body weight variation was more prominent for DMH treated rats, which successfully normalized by the treatment with VR24 and VR27 (Supplementary Fig. S3). A similar observation was measured for tumor incidence number and volume after treatment with both compounds. The test compounds and 5-FU significantly reduced ($p < 0.001$) the DMH-induced tumor volume up to three folds, compared to the CC group (Fig. 2A and B). On the other hand, Fig. 2C and D demonstrated pH and total acidity of colonic content in cancerous condition. After the DMH administration, we observed a significant decrease in colonic pH and increase in total acidity in DMH treated CC rats, as compared to the NC group. However, treatment with test compounds and 5-FU normalized these parameters and the effects were almost similar for both compounds and 5-FU (Fig. 2C and D).

The enzyme levels of AST, ALT, LDH, and ALP in the serum were measured in the similar experiment (Fig. 2E). All enzyme levels were increased in CC rats, compared to the NC. It was noted that the level of these enzymes was significantly ($p < 0.001$) attenuated after oral administration of VR24 and VR27 at both doses, compared to the CC rats.

3.2. Determination of oxidative stress parameters

Both compounds exhibited antioxidant effects in the CC rats (Table 1). Various oxidative stress parameters, including MDA, SOD, CAT, GSH and ProC in the colonic tissue were evaluated. There was a dramatic reduction for SOD in the CC group (~0.05) compared to the NC group (~0.17). Improvement in SOD level was observed up to 30–35% after treatment with VR24 and VR27. Again, we observed a reduction in GSH concentration in the CC group (~2.01 μM) with respect to the NC group (~3.10 μM). GSH level was improved after treatments with VR24 and VR27 (~3.0 μM) and this activity was almost similar to 5-FU. A similar trend was noted in CAT level with approximately 30% attenuation in the CC rats. The treatment with VR24 and VR27 significantly normalized the CAT level as showed in Table 1.

In addition, the formation of MDA and ProC were measured to evaluate the oxidative stress during CRC. The MDA formation was double in the CC rats (~0.17 nM), compared to the NC group (~0.09 nM). However, treatment with VR24 (~0.10 nM) and VR27 (~0.12 nM) at different doses attenuated the MDA formation. A similar observation was noted for ProC where the level of ProC was increased 40% in the CC rats and normalized after treatments.

3.3. Histopathology and SEM analysis of colon tissue

A number of lesions, epithelial stratifications, more vacuolated and damaged cells, goblet depletion, nuclear disparity and structural abnormality were observed in the colon tissue of CC rats after DMH treatment. Both VR24 and VR27 treatments repaired these structural abnormalities, shown in Fig. 3.

Further, SEM analysis showed similar trend where lesions of colon

Table 1
Effects of VR24 and VR27 after oral administration (10 and 25 mg/kg doses) on oxidative stress parameters in colon carcinogenic tissue for 15 days, respectively.

Groups	SOD (U/mg of Protein)	CAT mM H_2O_2 decomposed/min/mg of protein	GSH (μM/mg of Protein)	TBARS (nM of MDA/mg of protein)	ProC (μg/mg of protein)
NC	0.17 ± 0.04	11.32 ± 0.94	3.10 ± 0.42	0.09 ± 0.02	0.68 ± 0.15
CC (DMH)	0.05 ± 0.02	4.70 ± 2.62	2.01 ± 0.28	0.17 ± 0.02	1.10 ± 0.32
PC (DMH + 5-FU)	0.18 ± 0.01*	9.70 ± 0.77**	3.21 ± 0.74**	0.10 ± 0.01**	0.85 ± 0.30*
DMH + VR24 (10)	0.16 ± 0.03	8.68 ± 2.93*	3.12 ± 0.42*	0.11 ± 0.05**	0.88 ± 0.13*
DMH + VR24 (25)	0.20 ± 0.14*	9.23 ± 1.58**	3.05 ± 0.34*	0.08 ± 0.01***	0.89 ± 0.26
DMH + VR27 (10)	0.17 ± 0.01	9.03 ± 2.35*	3.12 ± 0.30*	0.10 ± 0.04**	0.85 ± 0.20*
DMH + VR27 (25)	0.18 ± 0.02*	9.54 ± 1.31**	3.19 ± 0.76**	0.08 ± 0.01***	0.88 ± 0.43*

Data represented as mean ± SD (n = 8). Statistically significant differences were observed between carcinogen control and test groups [one way-ANOVA followed by Bonferroni multiple comparison test. NC (Normal control), DMH (Carcinogen control: CC), DMH + 5-FU (Positive control: PC), DMH + VR24(10) (Treatment A10), DMH + VR24(25) (Treatment A25), DMH + VR27(10) (Treatment B10), and DMH + VR27(25) (Treatment B25).

* $p < 0.05$.
** $p < 0.01$.
*** $p < 0.001$.

tissue were more prominent in the CC rats, however, oral administration of VR24 and VR27 restored to normal architecture of colonic tissue (Fig. 3). The effects of VR24 and VR27 were found almost similar to that of the standard chemotherapeutics, 5-FU.

3.4. Effects of VR24 and V27 on IL-2, IL-6, COX-2 levels in the colonic tissue

Both compounds showed favorable effects on CRC-related inflammatory mediators in colon tissue. The normal concentrations of IL-2, IL-6 and COX-2 in rat colonic tissue increased up to 0.41, 2.03 and 1.52 folds, respectively, after DMH treatment in the CC rats (Table 2). VR24 and VR27 showed their ability to restore the concentrations of these mediators towards normal value.

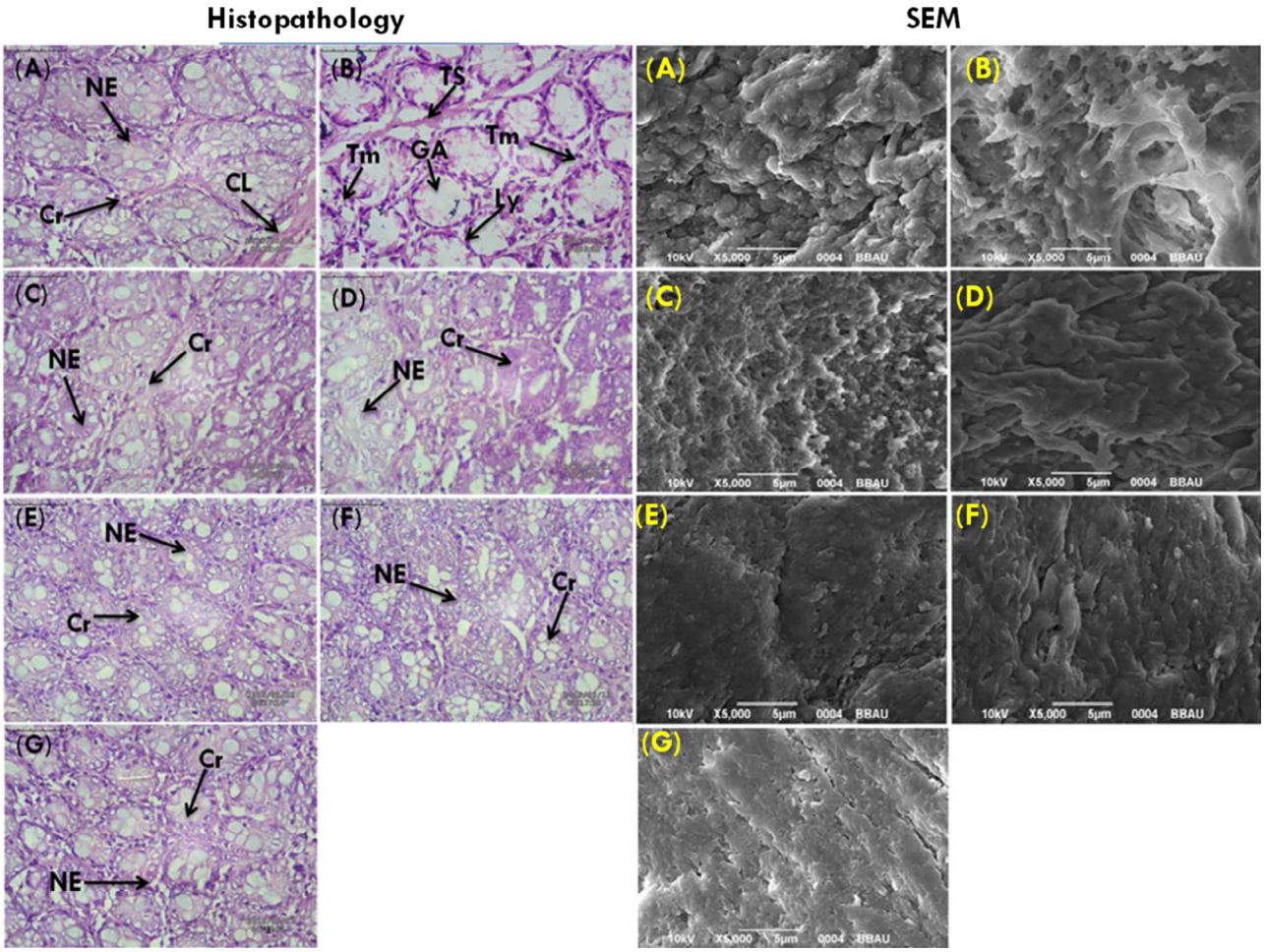

Fig. 3. The colonic pathological changes in DMH-induced CC rats (scale bar 50 μm) with 40X. Tumoral vacuoles were prominent in DMH group which was absent after 5-FU, VR24 and VR27 administration. (Cr – Crypts, NE – Normal epithelium, CL – Colon lumen, Tm – mucinous adenocarcinoma, GA – Goblet cell adinoma, Ly – Lymphatics (lined by endothelium), TS – Tumor stroma). (A) Normal control (NC), (B) DMH (CC), (C) DMH + 5-FU (PC), (D) DMH + VR24 (10), (E) DMH + VR24 (25), (F) DMH + VR27 (10) and (G) DMH + VR27 (25) groups.

Table 2
Effects of VR24 and VR27 on IL-2, IL-6, and COX-2 in colon carcinogenic tissue after oral administration of 10 and 25 mg/kg for 15 days, respectively.

Groups	COX-2 (pg/mL)	IL-2 (pg/mL)	IL-6 (pg/mL)
NC	706.30 ± 23.31	11.32 ± 0.94	485.14 ± 75.59
CC (DMH)	1076.21 ± 69.47	25.70 ± 1.62	989.0 ± 70.90
PC (DMH + 5-FU)	763.70 ± 55.65***	14.70 ± 0.77***	542.98 ± 73.42***
DMH + VR24 (10)	919.39 ± 63.22***	16.68 ± 2.93***	847.14 ± 76.00*
DMH + VR24 (25)	824.15 ± 13.96***	14.23 ± 1.58***	791.16 ± 91.01**
DMH + VR27 (10)	941.93 ± 69.70**	15.03 ± 2.35***	877.00 ± 71.32
DMH + VR27 (25)	887.82 ± 26.41***	13.54 ± 1.31***	834.08 ± 48.80*

Data represented as mean ± SD (n = 8). Statistically significant differences were observed between carcinogen control and test groups [one way-ANOVA followed by Bonferroni multiple comparison test.
* $p < 0.05$.
** $p < 0.01$.
*** $p < 0.001$.

3.5. mRNA expression of the effector cytokine IL-6, COX-2, JAK2 and STAT3 during DMH-induced CRC

To confirm gene expression levels of IL-6, COX-2, JAK2 and STAT3, we performed qRT-PCR analysis. The analysis showed the over-expression of these genes in DMH treated group, compared to the NC group. However, 5-FU, VR24 and VR27 administration normalized the overexpressed levels of these genes. The potency of VR24 and VR27 at 25 mg/kg was comparable to market available chemotherapeutics, 5-FU, without any significant difference (Fig. 4A).

3.6. Western blot analysis

The quantitative western blot analysis was employed to measure the protein expression levels of IL-6, COX-2, JAK2, p-JAK2, STAT3 and p-STAT3. The levels of IL-6 and COX-2 proteins were overexpressed in DMH induced carcinogen control group. It was observed that this overexpreesion was successfully inhibited after the treatment with VR24 and VR27. The protein levels of JAK2 and STAT3 were not significantly altered among different groups. However, the levels of p-JAK2 and p-STAT3 were dramatically over-expressed in DMH induced carcinogen control group and further suppressed after treatment with VR24 and VR27. The potency of VR24 and VR27 were found comparable or to some degree better than that of 5-FU (Fig. 4B).

3.7. Mathematical modeling of IL-6, COX-2 induced JAK2-STAT3 signaling pathway

The possible mechanism of VR24 and VR27 action towards the IL-6 and COX-2 mediated JAK2/STAT3 signaling blockade to protect tumor invasion is represented in Fig. 4C. Here, we made an attempt to formulate the dynamics of signal transduction pathway using a nonlinear mathematical model employing ordinary differential equations (ODEs). We started with a mathematical model of the JAK-STAT core module reflecting the sequential information transfer from cell membrane to nucleus and monitored activation/phosphorylation of STAT3 in response to dual stimulation of IL-6 and COX-2. The individual steps of the core module (Fig. 4C) were represented by a system of differential equations, each describing the dynamics of the different stages of STAT3 populations over time. In view of this, the basic feed forward model under consideration is,

$$\begin{aligned}
\frac{dx_1}{dt} &= -k_1x_1[IL{-}6]{-}k_1x_1[COX{-}2]\\
\frac{dx_2}{dt} &= -k_2x_2^2 + k_1x_1[IL{-}6] + k_1x_1[COX{-}2]\\
\frac{dx_3}{dt} &= -k_3x_3 + \frac{k_2}{2}x_2^2\\
\frac{dx_4}{dt} &= +k_3x_3
\end{aligned} \tag{1}$$

where [IL-6] and [COX-2] represent the amount of induced IL-6 and COX-2 respectively (obtained by quantitative western blot analysis) for different studied groups, $x_1$represents the amount of unphosphorylated STAT3 in cytoplasm, $x_2$is the amount of monomeric p-STAT3 in cytoplasm, $x_3$is amount of dimeric p-STAT3 in cytoplasm and $x_4$is the amount of dimeric p-STAT3 in the nucleus. k_1, $k_2$and $k_3$are the rate constants. Further, it was assumed that the individual reaction steps formulated by the ODEs in system (1) follow mass-action kinetics. Although this holds for the dimerization process, it represents an approximation for STAT3 phosphorylation and nuclear translocation. Moreover, it assumed that the tyrosine kinase, phosphorylating STAT3 monomers, and the nuclear transportation machinery are not rate limiting.

Typically, chemical reactions are reversible to some degree. To study the effect of the reversible nature of the chemical reaction from the dimer to the monomer, the second and third equations of system (1) are replaced by

$$\frac{dx_2}{dt} = -k_2x_2^2 + k_1x_1[IL{-}6] + k_1x_1[COX{-}2] + 2k_4x_3$$

$$\frac{dx_3}{dt} = -k_3x_3 + \frac{k_2}{2}x_2^2{-}k_4x_3$$

Thus, incorporating the reversible nature of chemical reaction, mathematical model represented by system of equations (1) is modified to

$$\begin{aligned}
\frac{dx_1}{dt} &= -k_1x_1[IL{-}6]{-}k_1x_1[COX{-}2]\\
\frac{dx_2}{dt} &= -k_2x_2^2 + k_1x_1[IL{-}6] + k_1x_1[COX{-}2] + 2k_4x_3\\
\frac{dx_3}{dt} &= -k_3x_3 + \frac{k_2}{2}x_2^2{-}k_4x_3\\
\frac{dx_4}{dt} &= +k_3x_3
\end{aligned} \tag{2}$$

where $k_4$is the backward reaction rate constant. To determine the quantitative behavior of STAT3 populations with time, ODEs given by (2) were integrated by 4th order Runge–Kutta method [37] using MATLAB software and the graphs were plotted (Fig. 5A–C). The numerical simulation was accomplished using the values of dynamical parameters k_1, k_2, $k_3$and $k_4$from the previous literature [16].

It is observed from Fig. 5A that the total amount of STAT3 in the cytoplasm exhibits a declining behavior in response to IL-6 and COX-2 stimulation. Further, it was observed that the declination was more rapid in carcinogen control group than those of the normal and treatment groups. Moreover, Fig. 5B revealed the behavior of STAT3 phosphorylation in cytoplasm, demonstrating that p-STAT3 in cytoplasm initially increased rapidly in response to dual stimulation of IL-6 and COX-2 but decreased again after prolonged times. The increase in the phosphorylation of STAT3 was found to be more pronounced in the carcinogen control group as compared to the normal and treatment groups. In addition, Fig. 5C manifests the quantitative behavior of all the STAT3 populations in response to the dual stimulation IL-6 and COX-2.

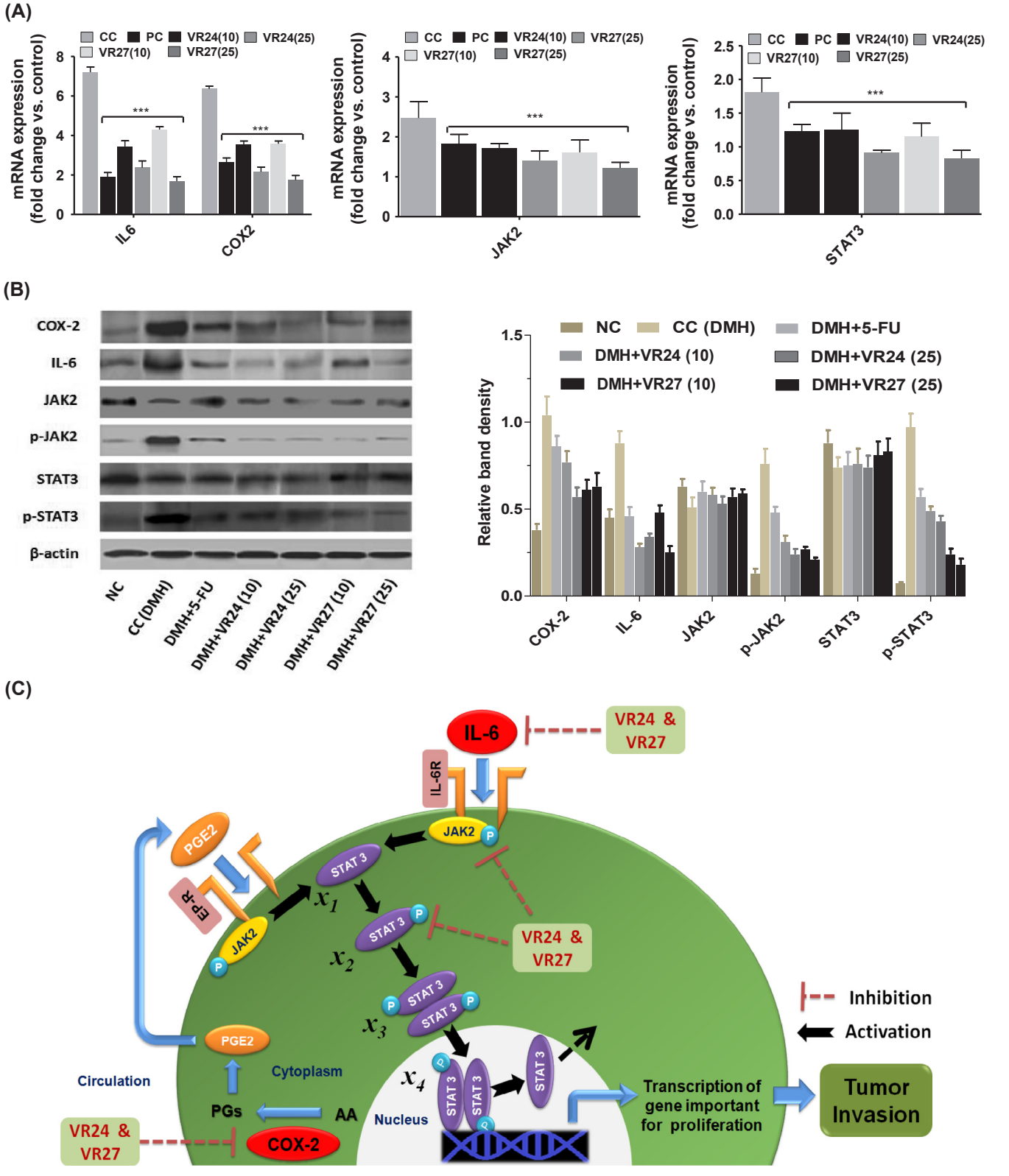

Fig. 4. (A) Gene expression levels of IL-6, COX-2, JAK2 and STAT3 after treatments with VR24 and VR27 (determined by qRT-PCR analysis). Data represented as mean ± SD (n = 8). Statistically significant differences were observed between CC and test groups [Paired *T*-test, (***p < 0.001)]. (B) The protein expression levels of COX-2, IL-6, JAK-2, p-JAK2, STAT3 and p-STAT3 in colon tissue after treatment with VR24 and VR27 (determined by quantitative western blot analysis). (C) The core module of the IL-6 and COX-2 induced JAK2/STAT3 pathway: Firstly, IL-6 secreted by cells of the innate or adaptive immune system binds to soluble IL6R. IL-6 binding to IL-6R results in tyrosine phosphorylation (P) of JAK2. Phosphotyrosine residues in the IL-6R mediate recruitment of monomeric STAT3 (x_1). Upon receptor recruitment, monomeric STAT3 is tyrosine phosphorylated (x_2) to form phosphorylated/activated STAT3. The activated p-STAT3 forms the dimers (x_3), which translocate to nucleus (x_4), bind to DNA and transcript several oncogenes to accelerate the tumor progression. Similarly, COX-2 catalyzed the production of prostaglandin E2 (PGE2) from arachidonic acid (AA), which binds to the epidermal growth factor receptor (EP-R) on the cell membrane and activates the JAK2, followed by the phosphorylation of STAT3. VR24 and VR27 could exert dual inhibitory effects on COX-2 and IL-6 mediated JAK2/STAT3 signaling pathways.

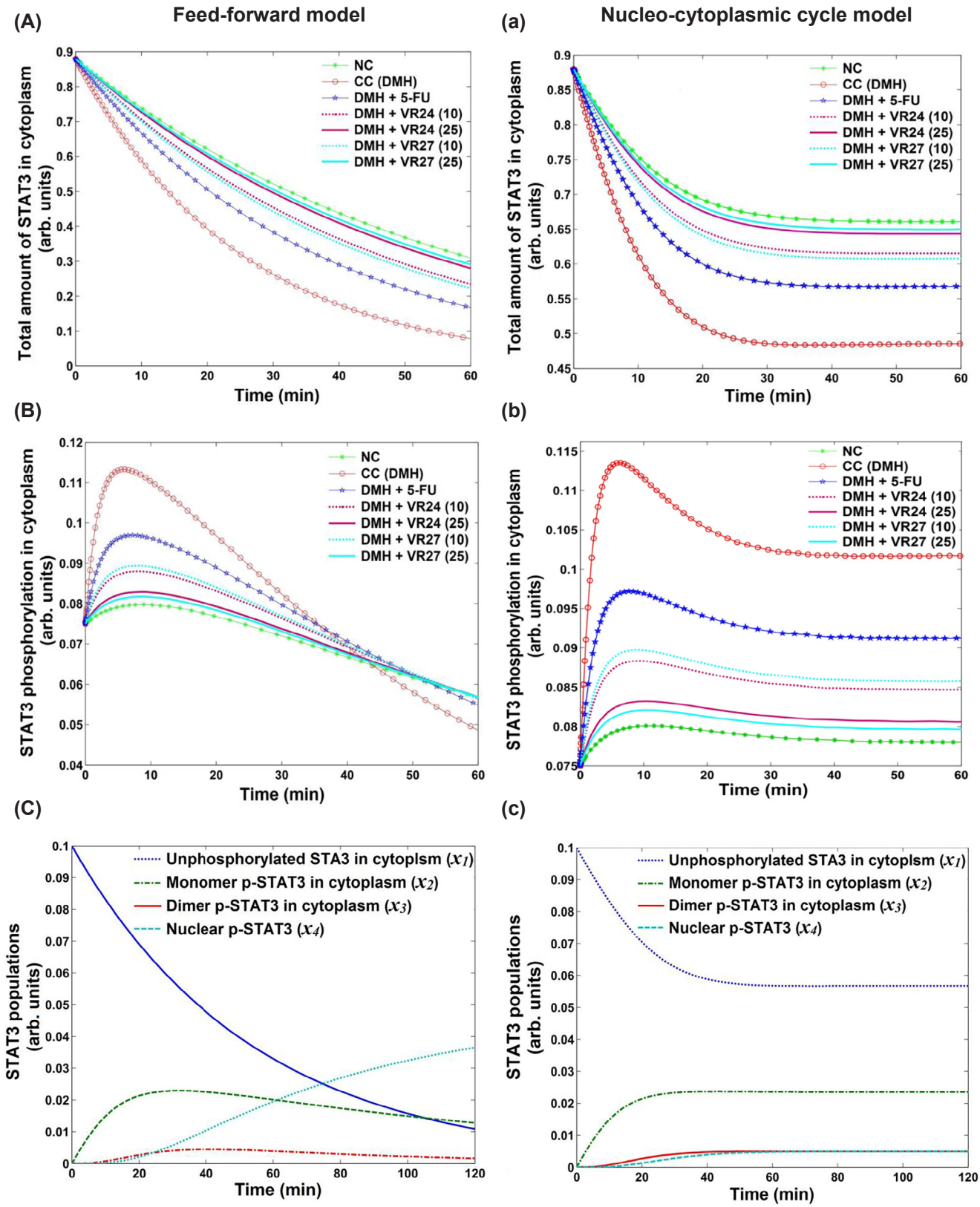

Fig. 5. Feed-forward model is represented by (A) (B) and (C) whereas Nucleo-cytoplasmic cycle model is shown by (a) (b) and (c). All of these graphs were generated through MATLAB software using the derived mathematical model based on the steps involved in the pathway. Graphs (A) and (a) show the quantitative behavior of total STAT3 in cytoplasm due to dual stimulation of IL-6 and COX-2. Similarly, Graphs (B) and (b) show the quantitative patterns of tyrosine phosphorylated STAT3 whereas graphs (C) and (c) show the quantitative behavior of all the STAT3 populations in response to dual stimulation of IL-6 and COX-2.

Previous literature suggests that the active role of STAT3 might not end in the nucleus. It could follow a feedback mechanism by reentering to the cytoplasm after dedimerization and dephosphorylation and thereby involved into another round of activation. Thus, considering the nucleo-cytoplasm cyclic nature of the pathway and reversibility of chemical reaction, we further modified system (2) as follows:

$$\begin{aligned}\frac{dx_1}{dt} &= -k_1x_1[IL{-}6]{-}k_1x_1[COX{-}2] + 2k_5x_4\\ \frac{dx_2}{dt} &= -k_2x_2^2 + k_1x_1[IL{-}6] + k_1x_1[COX{-}2] + 2k_4x_3\\ \frac{dx_3}{dt} &= -k_3x_3 + \frac{k_2}{2}x_2^2{-}k_4x_3\\ \frac{dx_4}{dt} &= +k_3x_3{-}k_5x_4\end{aligned} \quad (3)$$

where $k_5$is rate at which a dimer STAT3 reverts to the stage of monomer STAT3 in cytoplasm after its dedimerization and deactivation in nucleus. To study the dynamical behavior of STAT3 in different stages incorporating the nucleo-cytoplasm cyclic pathway, system (3) was again integrated through MATLAB software and graphs were plotted. The declining behaviour of STAT3 and elevating behavior of p-STAT3 over time in both the systems (2) and (3) were found similar initially. However, nucleo-cytoplasmic model attained a steady state after some time in contrary of the feed forward model. Further, it was observed that the behavior of STAT3 and p-STAT3 in both the systems demonstrated parallelism among all the groups. The pattern of variations in different STAT3 populations in system (2) and (3) within cellular environment over time is shown in Fig. 5(C) and (c), respectively in response to dual stimulation of IL-6 and COX-2.

3.8. ^{1}H NMR-based metabolomics to access the biochemical impact of VR24 and VR27

3.8.1. Spectral assignment

The 1D ^{1}H-CPMG NMR spectra acquired from serum samples of different control and treated rats, individually with the assigned resonances are shown in Fig. 6. The 1D ^{1}H-CPMG NMR spectra resonances of metabolites were assigned by comparing them with those of the reported data from HMDB [38] and BMRB database [32]. The ^{1}H NMR spectra showed signals mainly from lipids/lipoproteins i.e. low-density lipoprotein (LDL), high-density lipoprotein (HDL), very low-density lipoprotein (VLDL) and amino acids such as alanine, arginine, valine, leucine, isoleucine, histidine, tyrosine and glutamine. Other identified metabolites were glucose, glycerol, choline, creatine/creatinine, acetone, pyruvate, acetate, citrate, lactate, betaine, myo-inositol, malonate, N-acetyl glutamate (NAG), N-acetyl aspartate (NAA), 4-OH butyrate methionine etc.

3.8.2. Serum metabolic profiling using 1D ^{1}H NMR

Univariate and chemometrics statistical analysis were employed to investigate the DMH-induced metabolic alterations in CRC condition and reveal the protective effect of both VR24 and VR27 on this. Chemometrics analysis was performed using PCA to construct the score plots of each rat for an initial overview of the data set and identifying the outlier samples. There was no any outlier variant in each group. The combined and pairwise PCA score plots of all variants are shown in Fig. 7A and B. These results showed a clear trend of clustering in different groups. OPLS-DA model analysis of this subject was further carried out to minimize the feasible contribution of intergroup variability and to improve the better separation between each group. The individual score plot was measured between two groups, compared to the CC group (Fig. 7C). The results of OPLS-DA model analysis showed that both VR24 and VR27 exhibited a clear separation, compared to the CC group. The quality of these models showed a significantly higher quality of fit and predictability such as $R^2Y > 0.8$, $Q^2 > 0.2$. Furthermore, the OPLS-DA model was validated on the basis of permutation statistics using 100 permutations as shown in Supplementary Fig. S4. The model parameters for explaining variation (R^2Y) and the predictive capability (Q^2) were significantly high (displayed in their respective OPLS-DA score-plots, Supplementary Fig. S4) in each case, demonstrating that the pairwise OPLS-DA models assembled from CPMG spectra exhibited satisfactory fit with good discriminatory power. The careful assessment of combined OPLS-DA score plot also exposed that VR24 and VR27 treatments exerted the impact on DMH-induced CRC as deduced by the shift of the VR24 and VR27 treatment groups back towards getting closer to the NC group. The visual assessment of the pairwise score plots exhibited a clear separation between treated and CC groups, which showed significant metabolic alteration in DMH treatment. The variable metabolites were carefully selected when the statistically major threshold of variable influence on projection (VIP) values determined from the OPLS-DA model were larger than 1 as shown in Supplementary Table S2. These VIP scores of metabolites expressed a weighted sum of squares of the PLS loadings and took into account the amount of explained Y-variation in each dimension showing the effects of each metabolite in the model.

Further, the OPLS-DA loadings S-plot was derived from pairwise

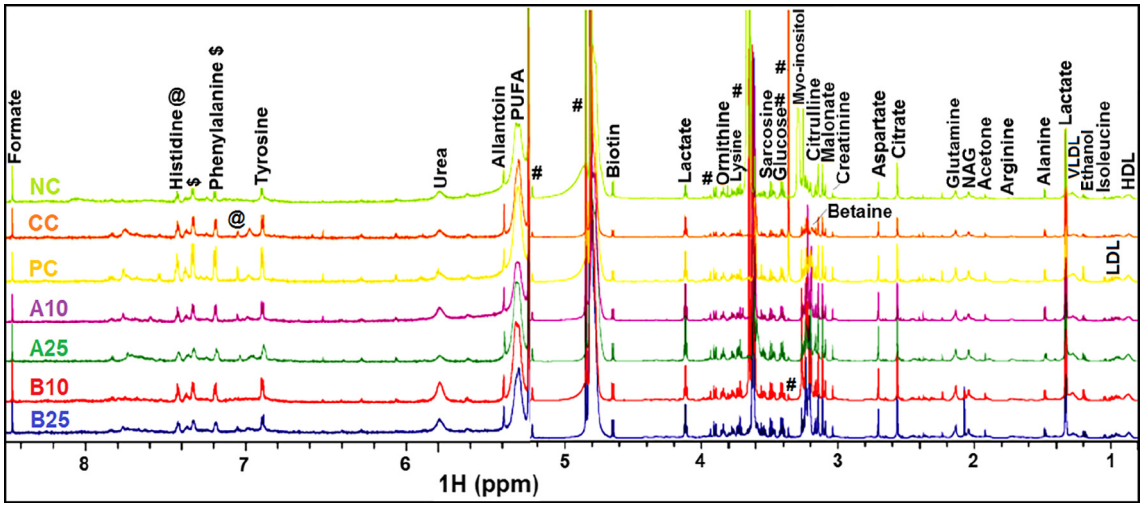

Fig. 6. Stack plot of representative 1D ^{1}H CPMG NMR spectra of rat serum obtained from different groups. ^{1}H NMR [($CDCl_3$, 800 MHz). NC (Normal control), DMH (Carcinogen control: CC), DMH + 5-FU (Positive control: PC), DMH + VR24(10) (Treatment A10), DMH + VR24(25) (Treatment A25), DMH + VR27(10) (Treatment B10), and DMH + VR27(25) (Treatment B25). The peaks annotated in the figure show the assignments of serum metabolites. The abbreviations used are: LDL/VLDL: Low/very-low density lipoproteins; HDL: high density lipoproteins; NAG: N-acetylglucosamine, His: Histidine.

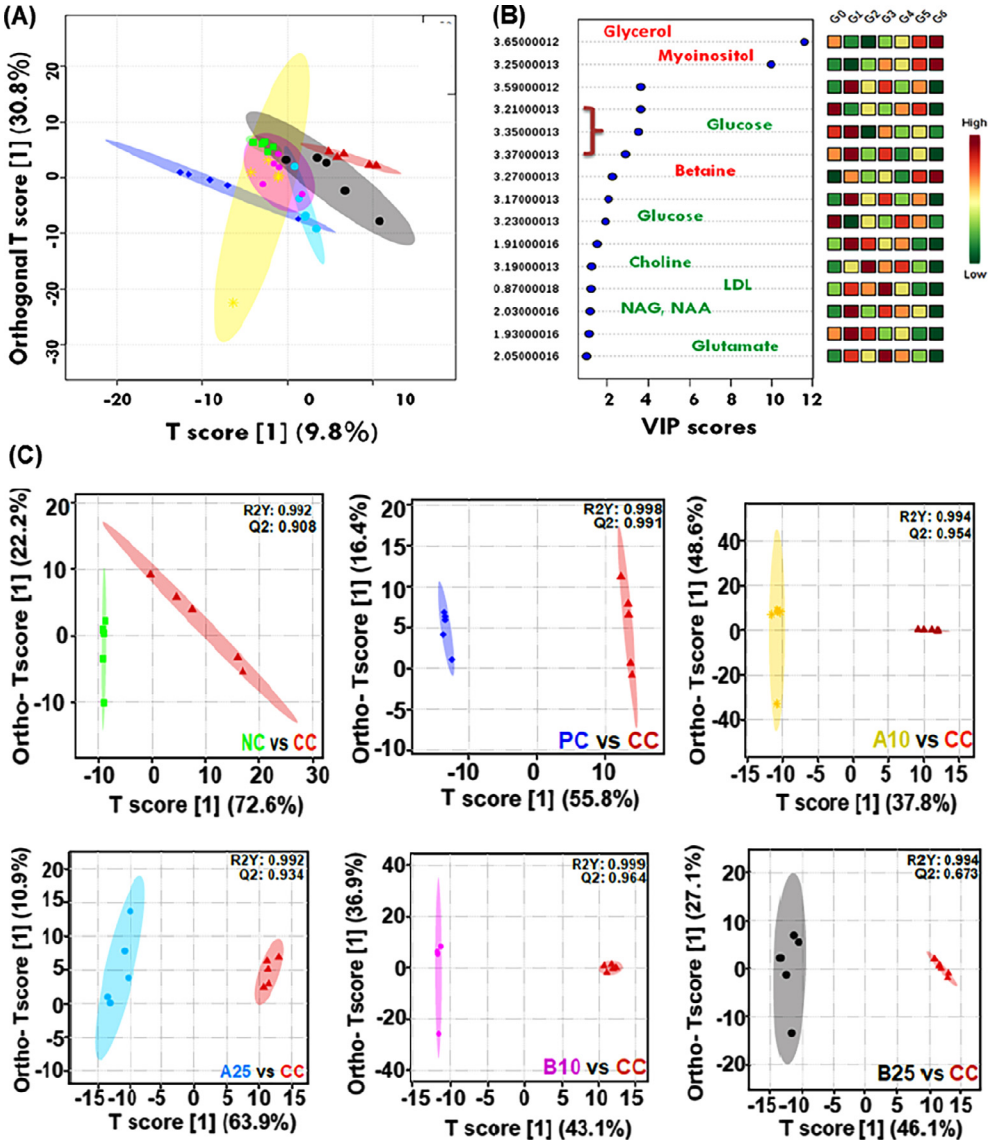

Fig. 7. Combined and pair-wise OPLS-DA analysis: (A) The 2D OPLS-DA analysis of 1D ^{1}H CPMG NMR spectra score plot derived from combined analysis comprising of all the groups: Normal control [NC] (G0), DMH + 5-FU [PC] (G1), DMH [CC] (G6), DMH + VR24 [10] (G2), DMH + VR24 [25] (G3), DMH + VR27 [10] (G4) and DMH + VR27 [25] (G5), pair-wise analysis. (B) The potential discriminatory metabolite entities identified from VIP scores derived from PLS-DA modeling of complete data matrix and resulted VIP scores for top 15 metabolite entities are shown in increasing order of VIP score values to highlight their discriminatory potential. (C) Represents the Combined score plots compromising of all the groups and CC score plots comprising with treatments group.

analysis that represents the combined score plots comprising of all the groups are shown in Supplementary Fig S5. The top region of resonance represents the up-regulation of discriminated metabolites besides the bottom of S-plot expressed the down-regulation of particular metabolites. The up and down-regulated metabolites of 5-FU, VR24, and VR27 treated groups, compared to the CC group, were quantitatively assessed using the box-cum-whisker plots from the OPLS-DA loadings S-plot (Fig. 8). In the box plots, the boxes denote interquartile ranges where horizontal line inside the box denotes the median, and bottom and top boundaries of boxes are 25th and 75th percentiles, respectively. Lower and upper whiskers are 5th and 95th percentiles, respectively. The results of quantitatively assessed metabolites study suggested that the myoinositol and glycine level up-regulated (approximately 30–40%) in the CC group. Besides, sarcosine, tryptophan and glucose showed the down-regulation (approximately 10–40%) in the CC group that were normalized after treatment with 5-FU, VR24 and VR27. Next, cluster analysis was performed to identify the intrinsic similarities in group where, it was observed that the number of variants in the particular groups showed the intrinsic similarities as illustrated in Supplementary Fig S6. Further, univariate analysis was performed to reduce a possibly bulky number of measured analytes. Each variable in the data having two groups (e.g. test and CC) was analyzed using student's *T*-test at three significant levels ($p \leq 0.05$, $p \leq 0.01$, and $p \leq 0.001$). All groups were compared with the CC rats as shown in Supplementary Table S2. Biomarker analysis was performed using classical univariate ROC curve analyses for individual biomarker identification. These models were validated by diagnostic parameters such as the number of cross-validated explained variation Q2, misclassifications, and the AUC of a receiver operating characteristic (ROC) analysis. Overall, we identified 35 metabolic markers extensively perturbed in NC, 5-FU, VR24 and VR27 treated rats, compared to the CC rats. These metabolic markers entities along with their chemical shifts, AUC, ROC, their levels (up or down levels) and students *T*-test at three significant levels ($p \leq 0.05$, $p \leq 0.01$, and $p \leq 0.001$) are listed in Supplementary Table S2. A significant increase in lipids, myoinositol, betaine and glycerol was noticed in the sera of CC rats, compared to the NC group. On the other side, there was a significant decrease in the levels of glucose, isoleucine, leucine, ethanol, VLDL, NAA, NAG, citrate, citrulline, malonate, choline and amino acids (glutamate, and glutamine) was observed in the CC group. The levels of all these metabolites restored to normal after VR24 and V27 administration, which showed the potential of these compounds towards metabolites regulation.

3.8.3. *Pathways analysis*

To understand the cellular process of these metabolites, it is essential to provide the insights into the metabolic pathways involving

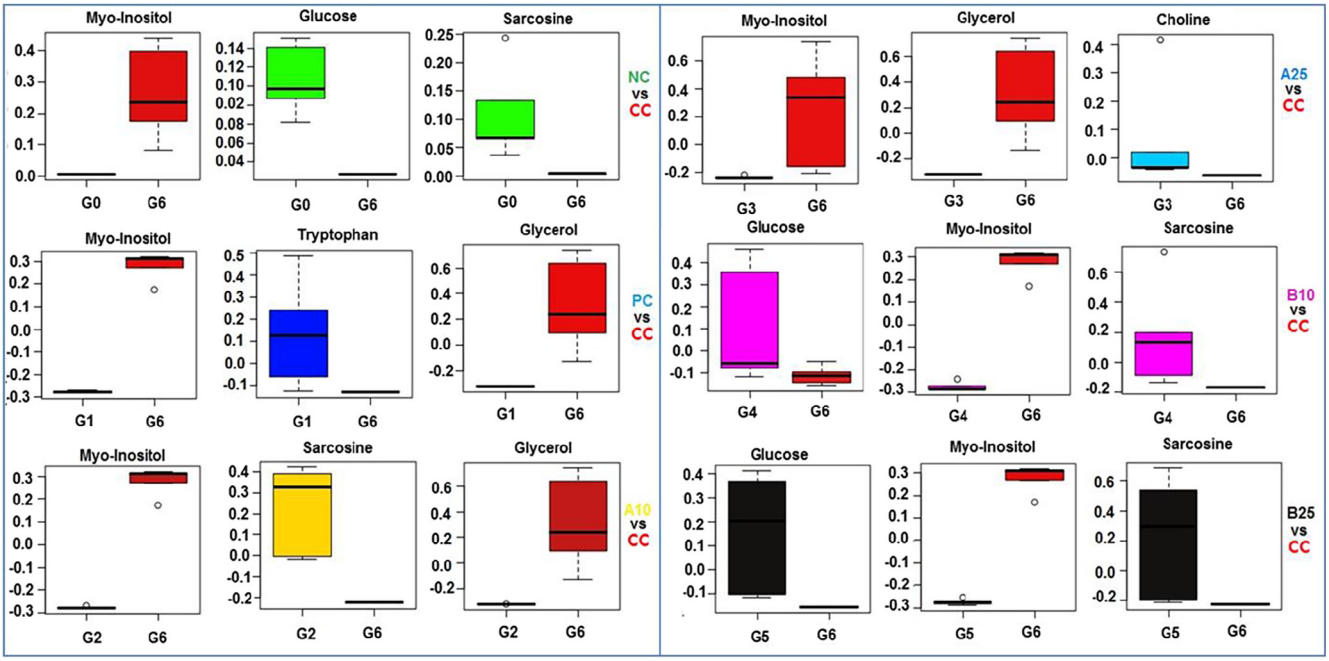

Fig. 8. Metabolic effects of VR24 and VR27 treatment: The box-cum-whisker plots are showing relative variations in quantitative profiles of serum metabolites relevant in the context of the pathophysiology of CRC. In the box plots, the boxes denote interquartile ranges, horizontal line inside the box denote the median, and bottom and top boundaries of boxes are 25th and 75th percentiles, respectively. Lower and upper whiskers are 5th and 95th percentiles, respectively. Normal control (NC) [G0], DMH (Carcinogen control: CC) [G6], DMH + 5-FU (Positive control: PC) [G1], DMH + VR24(10) (A10) [G2], DMH + VR24(25) (A25) [G3], DMH + VR27(10) (B10) [G4], and DMH + VR27(25) (B25) [G5].

these metabolites. After the identification of potential metabolites biomarkers, the particular pathways were constructed using databases such as KEGG, HMDB and the literatures related to pathway analysis of certain metabolites and cancer disease.

The major metabolic changes were identified during PLS-DA analysis using student T-test, which have the better VIP scores as shown in Supplementary Table S2. More significant metabolites were further subjected to determine the influenced metabolic pathways using pathway analysis module, a pathway topology analysis and the combination of enrichment analysis inbuilt in the MetaboAnalyst. The lipid and membrane metabolites such as VLDL, lipids, NAG and OAG were excluded in this pathways analysis.

The final list of more significantly altered metabolites was analyzed by Over-Representation Analysis (ORA) in MetaboAnalyst. The rat (*Rattus norvegicus*) pathway library, the out-degree centrality algorithms, and the hypergeometric test were used for pathway topology analysis and pathway enrichment analysis. The pathway analysis module afforded a fit coefficient (p) from pathway enrichment analysis with an impact factor from pathway topology analysis for each analyzed pathway. All matched pathways are expressed as per their *p*-values from the pathway enrichment analysis (vertical axis or y-axis, the intensity of color) and pathway impact values from pathway topology analysis (horizontal axis or x-axis, the size of circle), with the major impacted pathways colored in red. These impacts of pathway suggested the cellular function and possibilities of metabolites in the cellular process according to privileged pathways (Supplementary Fig. S7). The output of impact showing in pathway analysis helped to make a plausible metabolic pathway. In the proposed pathways, the red color showed the significant up-regulation of metabolites and green color represented the down-regulation of particular metabolites in the carcinogen control groups, compared to the NC group (Fig. 9). The results of these pathways indicated the role of enzymes which controls the levels of metabolites biomarker in the cell cycle and plays a critical role in the CRC development. Thus, these metabolites which are regulated by an enzyme in the cellular pathways might be helpful to understand the impact upon the cellular pathways and to explore the mechanisms associated to the CRC.

4. Discussion

CRC is the third most common cause of cancer deaths throughout the world [39]. The clinical outcome of CRC treatment remains limited due to severe adverse effects and tumor resistance towards marketed chemotherapeutics [40,41]. Thus, the major intension of our research group is to contribute new lead molecules for developing cancer therapeutics that could have greater effectiveness and prominent selectivity. In view of this, recently we rationally designed and synthesized novel 1,3,4-thiadiazole derivatives with prominent *in vitro* cytotoxicity against HT-29 human CRC cell line. Molecular docking study revealed that two compounds (VR24 and VR27) showed remarkable binding affinity and good stability of ligand-protein complex with various CRC-related pro-inflammatory targets IL-2, IL-6 and COX-2 [14].

In the present context, we performed acute toxicity studies of our newly synthesized compounds at 5, 10 and 25 mg/kg for 15 days in albino Wistar rats. Both compounds were found safe in experimental *in vivo* rat model up to a dose of 25 mg/kg dose. Pharmacokinetic parameters described in our previous literature showed optimal levels of oral absorption, plasma distribution and renal clearance of VR24 and VR27 [15]. In the present context, CRC condition was developed by the administration of DMH in albino Wistar rats. The DMH-exposure altered various physiological parameters, including increase in body weight, tumor volume, incidence number and decreased in pH. These altered parameters were restored after administration of VR24 and VR27 at 10 and 25 mg/kg and standard chemotherapeutics, 5FU, at 10 mg/kg for 15 days, showing anti-proliferative effects of these compounds on this model. Simultaneously, DMH-exposure showed its ability to damage liver during CRC condition as evidenced through the increased concentration of various liver function enzymes ALT, AST, LDH and ALP in serum [42,43]. Treatment with VR24 and VR27 reduced these hepatic enzyme levels near to normalcy, showing their protective action. Anti-CRC action was further evaluated *via* measurement of oxidative stress parameters in colonic tissue. It is well established that GSH acts as a free radical scavenger and protects against the oxidative damage [44,45]. Decrease in GSH level showed oxidative

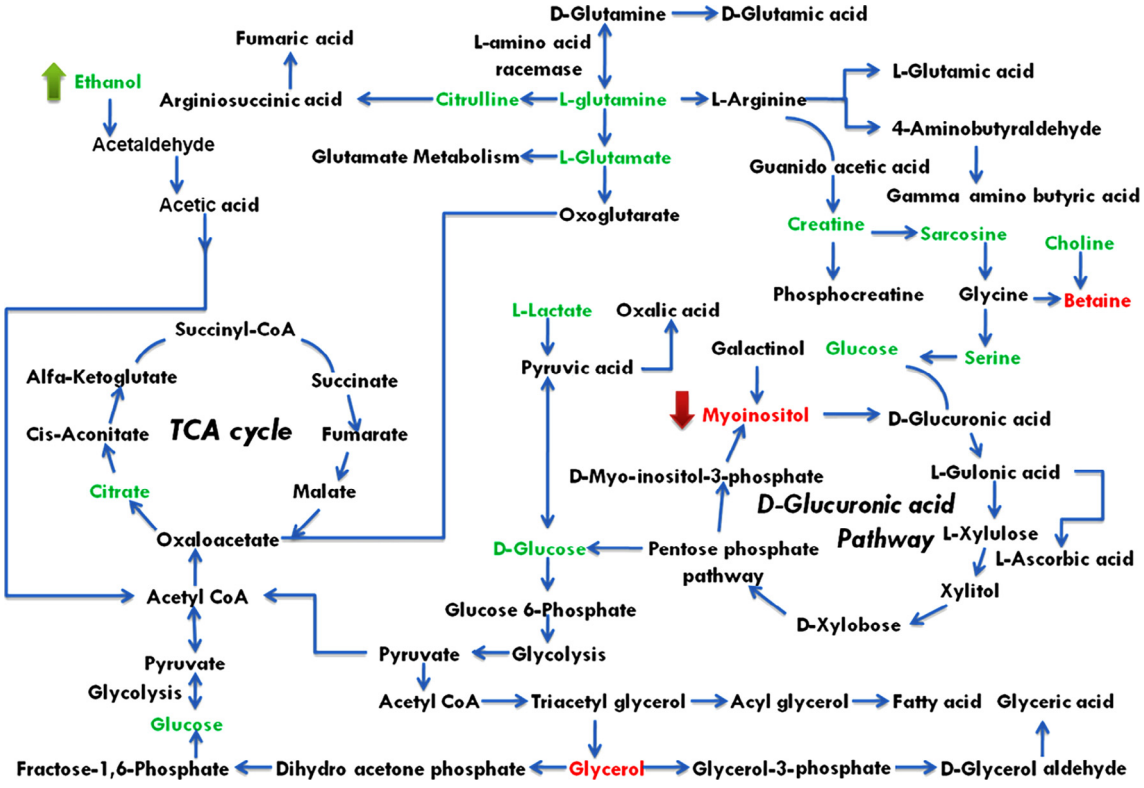

Fig. 9. Major interlinking metabolic pathways (glycolysis, TCA cycle, inositol metabolomics, amino-acids and D-glucuronic acid pathways), which consist of the major metabolites perturbated in CRC condition and restored after treatments with VR24 and VR27. Green color: decrease in particular metabolites concentration in carcinogen control group that was restored after VR24 and VR27 treatments. Red color: increase in particular metabolites concentration in carcinogen control group that was restored after VR24 and VR27 treatments.

damage of colonic tissue during CRC condition. The treatment with VR24 and VR27 restored the decreased level of GSH to normal. In addition, SOD and CAT are the antioxidant enzyme that neutralize superoxide's free radicals and convert hydrogen peroxide into water and oxygen, respectively [22]. Treatment with 5-FU and both compounds increased CAT and SOD levels in colonic tissue. The increase in the concentrations of these antioxidant markers in the treatment groups showed the antioxidant effect of both compounds during CRC conditions. Oxidation of protein and lipid to corresponding MDA and ProC is another important aspect to be measured during CRC condition. This study corroborated well with previous report [22] that showed an elevation in both MDA and ProC level in DMH-treated rats. These concentrations were decreased after administration of V24 and V27 in the CRC tissue, showing potential anti-oxidant effects in CRC. Altogether, it might be concluded that both V24 and V27 exhibited the ability to reduce oxidative stress induced damage during CRC.

Furthermore, the histopathological examination and SEM analysis confirmed the protective effects of both compounds against CRC. In CRC condition, histopathology and SEM analyses revealed the formation of tumoral vacuoles and tumoral stroma in the colonic tissue of DMH-treated rats [22]. Both VR24 and VR27 abolished tumoral vacuoles in CRC tissue and showed normal architecture of tissue, indicating the antiproliferative effect of these compounds. SEM analysis again confirmed the protective actions of both compounds where damage in colonic tissue was restored to normal after treatment.

To explore the molecular insights into the mechanism of anti-CRC action of these compounds, we focused our attention on various CRC-related pro-inflammatory targets. It has been observed that various proinflammatory cytokines such as IL-2, IL-6 or COX-2 are over-expressed at inflammatory sites of CRC [12,46]. Several studies have suggested that the overexpression of cytokines can mediate the cascade amplification of inflammation responsible for the initiation and progression of CRC [4]. Consequently, we measured the concentration of these proinflammatory markers by ELISA assay. Data obtained from ELISA corroborated well with previous observation where IL-2, IL-6 and COX-2 concentrations were elevated in DMH treated rats [14]. These elevations restored near to normal values after treatment with VR24 and VR27. A lesser reduction in IL-6 level was observed in VR24 and VR27 treated groups when compared to 5-FU treated group. However, the effects of treatment with VR24 and VR27 on IL-6 level were noted in a dose dependent manner. Further, qRT-PCR analysis substantiated the previous findings where the mRNA levels of IL-6, COX-2, JAK2 and STAT3 were over-expressed at tumorigenic sites. Treatment with VR24 and VR27 inhibited this overexpression that rendered their ability to show the suppressive action of these genes at molecular level.

Moreover, it is well documented that IL-6 and COX-2 serves as a JAK2/STAT3 activator [4] and thereby CRC progression. IL-6 stimulation is mediated through various oncogenic agents that leads to the activation of JAK2 followed by phosphorylation/activation of STAT3 [47,48]. This activated STAT3 undergoes homo/hetero dimerization followed by nuclear translocation, DNA binding, and transcription of various oncogenes [47,48]. Consequent with this information, western blot assay showed over-expression of IL-6, COX-2, p-JAK2 and p-STAT3 proteins in DMH-treated CRC group indicating CRC pathogenesis. The overexpression in the levels of these proteins was successfully down-regulated after treatment with VR24 and VR27, particularly at 25 mg/kg dose. However, there were not any significant changes observed in the levels of JAK2 and STAT3 proteins. This observation indicated that the IL-6 and COX-2 mediated activation of JAK2/STAT3 was due to the enhanced phosphorylation of JAK2/STAT3. The result from western blot analysis explained that the anti-CRC effects of VR24 and VR27 was probably due to the inhibition of IL-6 and COX-2 mediated activation/phosphorylation of JAK2/STAT3.

Mathematical modeling is another approach in the field of molecular biology. Interestingly, it constitutes a system of differential equations formulated for the natural phenomenon occurring in a

particular pathway [49]. In view of this, we employed the approach of mathematical modeling and formulated four ODEs describing the natural process of IL-6 and COX-2 induced JAK2-STAT3 pathway. Now, we used the quantitative values of IL-6 and COX-2 for different studied groups into the system of ODEs. Further, the dynamic behavior of phosphorylation, dimerization and nuclear translocation of STAT3 over a definite time course were identified using MATLAB software. It was observed that the equilibrium level of p-STAT3 is greater in carcinogen control group as compared to those of the normal and treatment groups. This implies that the enhanced phosphorylation of STAT3 causes the development of CRC condition which, in turn, can be treated with VR24 and VR27 administrations. Through mathematical modeling, it has also been observed that the phosphorylation of STAT3 is mediated by the dual stimulation of IL-6 and COX-2 in our experiment. Importantly, the mathematical modeling provided following additional information; (1) mathematical modeling provided the authenticity of our experimental findings by showing the similarity in the patterns of STAT3 phosphorylation, (2) applying the fitted models, we predicted the quantitative behavior of different STAT3 populations (monomer STAT3, p-STAT3, dimer p-STAT3 in the cytoplasm and dimer p-STAT3 in the nucleus) over a time course that is not directly accessible to western blot analysis, (3) dynamic model of IL-6 and COX-2 mediated JAK/STAT signaling pathway can promote a functional understanding at the system level. Thus, the combined approach of quantitative western blot analysis and data-based mathematical modeling provided a deep understanding of this pathway. This also revealed the molecular basis of VR24 and VR27 action through the dual inhibition of IL-6 and COX-2 mediated phosphorylation/activation of JAK2/STAT3. Altogether, this observation clearly explained that these compounds showed capacity to block IL-6 and COX-2 mediated JAK2/STAT3 molecular pathway.

^{1}H NMR-based metabolomics analysis provides the more discriminable signature and quantitative information of metabolites in CRC condition and after treatments [50]. The identification and characterization of perturbed metabolites in CRC may play a significant role in the early diagnosis and therapy. It helps to make the possible map for the drug action into metabolomic pathways in CRC condition [51]. To the best of our knowledge, we are reporting the impact of 1,3,4-thiadiazole derivatives in CRC using ^{1}H NMR-based serum metabolomics for the first time. This study coupled with multivariate statistical data analysis to investigate the DMH-induced metabolic alterations and to assess the ameliorative effects of VR24 and VR27 treatment on these alterations. The CRC associated metabolic pathway involves amino acids, ketone body, choline metabolism, glycolysis, TCA cycle, phosphatidylinositol, and neoglucogenesis [52,53]. We observed a significant decrease in glucose level in the CC group, compared to the NC group, indicating enhanced glycolytic pathway and more glucose uptake by CRC tissue for cellular proliferation. These findings were fully corroborated with previous observations explaining War-burg effect and may be linked to lower amount of glucose utilization by cancerous tissues [54].

In addition, myoinositol is also a constituent of cell membranes which releases phosphate ions in serum and thereby increases the adenosine triphosphate (ATP) formation and cell cycle [55,56]. Treatment with VR24 and VR27 normalized the altered level of myoinositol, signifying their antiproliferative potential. Glycerol is the major by-product of lipid metabolism which is raised in the body during CRC condition [52,53]. We found the higher amount of glycerol in the serum of CRC rats, demonstrating increased lipid metabolism in cancerous condition [52,53]. Treatment with 5-FU, VR24 and VR27 decreased the level of glycerol in serum, indicating the ability of these compounds to enhance the glycerol metabolism.

In addition, betaine was upregulated in serum and over production of betaine causes tumor progression [57]. Treatment with both compounds normalized betaine concentration that indicated their protective effects in CRC. NAG has anti-inflammatory effect that is generally down-regulated in CRC condition [58,59]. Treatment with VR24 and VR27 restored the altered level of NAG to normal, signifying the capability of these compounds to inhibit inflammatory conditions during CRC. Furthermore, glutamate is the byproduct of glutamine, a precursor of GSH synthesis. GSH serves as natural antioxidant and free radical scavenger in oxidative degradation of cells [60,61]. Concentration of glutamine was decreased in the CRC rats during oxidative damage and recovered after treatment with VR24 and VR27 perhaps due to the antioxidant effects of these compounds. Lastly, choline and *O*-acetyl choline are the important constituent of cell membrane formation [60,61]. The levels of these metabolites were increased in the CRC rats, indicating higher rate of cell membrane formation with enhanced integrity. Both VR24 and VR27 normalized the concentration of these metabolites that exhibit the protective action of both compound during CRC.

Consequently, according to VIP scores of significant metabolites, the map of metabolomic pathways was constructed. The correlation between metabolites and amino acids was developed with respect to the CC groups. The DMH treated group showed higher rates of aerobic glycolysis, fatty acid synthesis, and tricarboxylic acid (TCA) cycle. This indicated high energy and biomass demands along with altered enzyme activities involved in tumor growth. Treatment with VR24 and VR27 significantly normalized the concentrations of almost all the metabolites, lipids and amino acids associated to these specific pathways. These metabolites modulation indicated perturbed energy metabolism of tumor cell and normalized after treatment with VR24 and VR27. Altogether, NMR-based metabolomics suggested the potential of these compounds to balance the abnormal metabolic pathways linked to fast growing tumor cells in CRC.

Conclusion

Although the mortality of CRC patients has been decreased by advances in colonoscopy, it remains the fourth leading cause of cancer-related death worldwide due to metastasis to other organs. As per the current demand in structural modification in 1,3,4-thiadiazoles, we recently synthesized novel 1,3,4-thiadiazole derivatives and discovered herein the cellular functioning of these compounds towards the CRC treatment at molecular level. Current study supported a clear link among biochemical, pathophysiological, molecular and metabolic parameters after treatment with VR24 and VR27. The molecular insights observed in this study could explain the role of these compounds in CRC treatment through the suppression of IL-6 and COX-2 mediated JAK2/STAT3 signals. The combined approach of quantitative western blot and mathematical modeling revealed that VR24 and VR27 have potential to inhibit the IL-6 and COX-2 mediated phosphorylation/activation of STAT3. Interestingly, the data-based mathematical modeling predicted the quantitative behavior of different STAT3 populations (cytoplasmic STAT3, cytoplasmic p-STAT3, cytoplasmic dimer p-STAT3 and their nuclear translocation) in response to IL-6 and COX-2 stimulations over a time course in both feed-forward as well as nucleo-cytoplasmic model. These quantitative behaviors can not be accessible through western blot analysis alone. Further, the *in vivo* findings of the present study confirm our recently reported *in vitro* findings. Finally, using a metabolomic approach in experimental *in vivo* model, we discovered herein the advance mechanistic understanding of their metabolic regulation that can prove the evidence of their cellular functioning. Therefore, we may conclude that VR24 and VR27 exhibited anti-CRC effect via the blockade of IL-6 and COX-2 mediated JAK2 and STAT3 signaling pathway.

Conflict of interests

The authors declare that they have no conflict of interests.

Acknowledgements

Dr. Sudipta Saha would like to express his thanks to the University Grants Commission (UGC), New Delhi, India, for UGC-MRP grant [Project no. 42-680/2013(SR)] and Department of Science and Technology (DST), India for DST-SERB project (Ref. No. DST/SB/EMEQ-320/2014). The authors would like to express their gratitude to Babasaheb Bhimrao Ambedkar University (BBAU), Lucknow, India for providing the support and research facilities. The authors also express their sincere gratitude to Centre of Biomedical Research (CBMR), Lucknow for providing the NMR facilities.

Appendix A. Supplementary material

Supplementary data associated with this article can be found, in the online version, at https://doi.org/10.1016/j.cyto.2018.03.026.

References

[1] G. Xu, G. Ren, X. Xu, H. Yuan, Z. Wang, L. Kang, et al., Combination of curcumin and green tea catechins prevents dimethylhydrazine-induced colon carcinogenesis, Food Chem. Toxicol. 48 (2010) 390–395.
[2] G. Iguchi, K. Chrysovergis, S.-H. Lee, S.J. Baek, R. Langenbach, T.E. Eling, A reciprocal relationship exists between non-steroidal anti-inflammatory drug-activated gene-1 (NAG-1) and cyclooxygenase-2, Cancer Lett. 282 (2009) 152–158.
[3] T. Shoji, H. Konno, T. Tanaka, T. Sakaguchi, K. Sunayama, M. Baba, et al., Orthotopic implantation of a colon cancer xenograft induces high expression of cyclooxygenase-2, Cancer Lett. 195 (2003) 235–241.
[4] S.-W. Wang, Y.-M. Sun, The IL-6/JAK/STAT3 pathway: potential therapeutic strategies in treating colorectal cancer, Int. J. Oncol. 44 (2014) 1032–1040.
[5] M. Wei, K. Morimura, H. Wanibuchi, J. Shen, K. Doi, M. Mitsuhashi, et al., Chemopreventive effect of JTE-522, a selective cyclooxygenase-2 inhibitor, on 1, 2-dimethylhydrazine-induced rat colon carcinogenesis, Cancer Lett. 202 (2003) 11–16.
[6] S. Maddila, S. Gorle, C. Sampath, P. Lavanya, Synthesis and anti-inflammatory activity of some new 1,3,4-thiadiazoles containing pyrazole and pyrrole nucleus, J. Saudi Chem. Soc. 20 (2016) S306–S312.
[7] F.A. Ragab, H.I. Heiba, M.G. El-Gazzar, S.M. Abou-Seri, W.A. El-Sabbagh, R.M. El-Hazek, Synthesis of novel thiadiazole derivatives as selective COX-2 inhibitors, Med. Chem. Comm. 7 (2016) 2309–2327.
[8] V. Raj, A. Rai, S. Saha, Human Cancer Cell Line Based Approach of 1, 3, 4-thiadiazole and its Fused Ring: A Comprehensive Review, Anti-Cancer Agents Med. Chem. 17 (2017) 500–523.
[9] H.P. Rang, M.M. Dale, J.M. Ritter, P.K. Moore, Pharmacology Churchill Livingstone, New York, 2003, pp. 3–4.
[10] J.M. Carethers, Systemic treatment of advanced colorectal cancer: tailoring therapy to the tumor, Therap. Adv. Gastroenterol. 1 (2008) 33–42.
[11] B. Chibaudel, C. Tournigand, T. Andre, A. de Gramont, Therapeutic strategy in unresectable metastatic colorectal cancer, Ther. Adv. Med. Oncol. 4 (2012) 75–89.
[12] T. Ohta, M. Takahashi, A. Ochiai, Increased protein expression of both inducible nitric oxide synthase and cyclooxygenase-2 in human colon cancers, Cancer Lett. 239 (2006) 246–253.
[13] S. Zha, V. Yegnasubramanian, W.G. Nelson, W.B. Isaacs, A.M. De Marzo, Cyclooxygenases in cancer: progress and perspective, Cancer Lett. 215 (2004) 1–20.
[14] V. Raj, A. Rai, A.K. Singh, A.K. Keshari, P.H. Trivedi, B. Ghosh, et al., Discovery of Novel 2-Amino-5-(Substituted)-1, 3, 4-Thiadiazole Derivatives: New Utilities for Colon Cancer Treatment, Anti-Cancer Agents Med. Chem. (2017), http://dx.doi.org/10.2174/1871520617666170419122916.
[15] V. Raj, A. Rai, A.K. Singh, A.K. Keshari, S. Saha, Pharmacokinetics studies of single orally administered 1,3,4-thiadiazoles: Method development and validation, Int. J. Pharmacokinet. 2 (2017), http://dx.doi.org/10.4155/ipk-2017-0006.
[16] I. Swameye, T.G. Muller, J. Timmer, O. Sandra, U. Klingmuller, Identification of nucleocytoplasmic cycling as a remote sensor in cellular signaling by databased modeling, Proc. Natl. Acad. Sci. U.S.A. 100 (2003) 1028–1033.
[17] J. Timmer, T.G. Muller, I. Swameye, O. Sandra, U. Klingmuller, Modeling the nonlinear dynamics of cellular signal transduction, Int. J. Bifurc. Chaos 14 (2004) 2069–2079.
[18] OECD Guideline for the testing of chemicals, Guidance document on acute oral toxicity. Environmental health and safety monograph series on testing and assessment, 2008, pp. 1–27.
[19] R.A. Furtado, B.R. Oliveira, L.R. Silva, S.S. Cleto, C.C. Munari, W.R. Cunha, et al., Chemopreventive effects of rosmarinic acid on rat colon carcinogenesis, Eur. J. Cancer Prev. 24 (2015) 106–112.
[20] R.A. Furtado, E.P. Rodrigues, F.R.R. Araujo, W.L. Oliveira, M.A. Furtado, M.R.B. Castro, et al., Ursolic acid and oleanolic acid suppress preneoplastic lesions induced by 1,2-dimethylhydrazine in rat colon, Toxicol. Pathol. 36 (2008) 576–580.
[21] M. El-Malt, W. Ceelen, C. van den Broecke, C. Cuvelier, S. Van Belle, W. De Neve, et al., Healing of experimental colonic anastomoses: effects of combined preoperative high-dose radiotherapy and intraperitoneal 5-fluorouracil, Int. J. Cancer 96 (2001) 297–304.
[22] A.K. Sahdev, V. Raj, A.K. Singh, A. Rai, A.K. Keshari, A. De, et al., Ameliorative effects of pyrazinoic acid against oxidative and metabolic stress manifested in rats with dimethylhydrazine induced colonic carcinoma, Cancer Biol. Ther. 18 (2017) 304–313.
[23] W. Kim, S.L. Flamm, A.M. Di Bisceglie, H.C. Bodenheimer, Serum activity of alanine aminotransferase (ALT) as an indicator of health and disease, Hepatology 47 (2008) 1363–1370.
[24] P.S. Kushwaha, V. Raj, A.K. Singh, A.K. Keshari, S.A. Saraf, S.C. Mandal, et al., Antidiabetic effects of isolated sterols from Ficus racemosa leaves, RSC Adv. 5 (2015) 35230–35237.
[25] N. Schaefer, K. Tahara, M. Von Websky, S. Wehner, T. Pech, R. Tolba, et al., Role of resident macrophages in the immunologic response and smooth muscle dysfunction during acute allograft rejection after intestinal transplantation, Transpl. Int. 21 (2008) 778–791.
[26] K. Magierowska, M. Magierowski, M. Hubalewska-Mazgaj, J. Adamski, M. Surmiak, Z. Sliwowski, et al., Carbon monoxide (CO) released from tricarbonyldichlororuthenium (II) dimer (CORM-2) in gastroprotection against experimental ethanol-induced gastric damage, PloS one 10 (2015) e0140493.
[27] X.-L. Wang, C.-M. Qiao, J.-O. Liu, C.-Y. Li, Inhibition of the SOCS1-JAK2-STAT3 signaling pathway confers neuroprotection in rats with ischemic stroke, Cell. Physiol. Biochem. 44 (2017) 85–98.
[28] A. Peinnequin, C. Mouret, O. Birot, A. Alonso, J. Mathieu, D. Clarencon, et al., Rat pro-inflammatory cytokine and cytokine related mRNA quantification by real-time polymerase chain reaction using SYBR green, BMC immunol. 5 (2004) 3.
[29] S. Han, A.J. Jeong, H. Yang, K.B. Kang, H. Lee, E.H. Yi, et al., Ginsenoside 20 (S)-Rh2 exerts anti-cancer activity through targeting IL-6-induced JAK2/STAT3 pathway in human colorectal cancer cells, J. Ethnopharmacol. 194 (2016) 83–90.
[30] H. Sui, S. Zhou, Y. Wang, X. Liu, L. Zhou, P. Yin, et al., COX-2 contributes to P-glycoprotein-mediated multidrug resistance via phosphorylation of c-Jun at Ser63/73 in colorectal cancer, Carcinogenesis 32 (2011) 667–675.
[31] D.S. Wishart, D. Tzur, C. Knox, R. Eisner, A.C. Guo, N. Young, et al., Querengesser, HMDB: the Human Metabolome Database, Nucleic Acids Res. 35 (2007) D521–D526.
[32] E.L. Ulrich, H. Akutsu, J.F. Doreleijers, Y. Harano, Y.E. Ioannidis, et al., BioMagResBank, Nucleic Acids Res. 36 (2007) D402–D408.
[33] J. Xia, N. Psychogios, N. Young, D.S. Wishart, MetaboAnalyst: a web server for metabolomic data analysis and interpretation, Nucleic Acids Res. 37 (2009) W652–W660.
[34] J. Xia, I.V. Sinelnikov, B. Han, D.S. Wishart, MetaboAnalyst 3.0–making metabolomics more meaningful, Nucleic Acids Res. 43 (2015) W251–W257.
[35] F. Puig-Castellvi, I. Alfonso, B. Pina, R. Tauler, 1H NMR metabolomic study of auxotrophic starvation in yeast using Multivariate Curve Resolution-Alternating Least Squares for Pathway Analysis, Sci. Rep. 6 (2016) 30982.
[36] Y. Quan-Jun, B. Jun, W. Li-Li, H. Yong-Long, L. Bin, Y. Qi, et al., NMR-based metabolomics reveals distinct pathways mediated by curcumin in cachexia mice bearing CT26 tumor, RSC Adv. 5 (2015) 11766–11775.
[37] S.A. Teukolsky, B.P. Flannery, W.H. Press, W.T. Vetterling, Numerical recipes in C. SMR 693, 1992.
[38] D.S. Wishart, D. Tzur, C. Knox, R. Eisner, A.C. Guo, N. Young, et al., HMDB: the human metabolome database, Nucleic Acids Res. 35 (2007) D521–D526.
[39] F.A. Haggar, R.P. Boushey, Colorectal cancer epidemiology: incidence, mortality, survival, and risk factors, Clin. Colon Rectal Surg. 22 (2009) 191–197.
[40] T.R. Asmis, L. Saltz, Systemic therapy for colon cancer, Gastroenterol. Clin. North Am. 37 (2008) 287–295.
[41] J.A. Meyerhardt, R.J. Mayer, Systemic therapy for colorectal cancer, N. Engl. J. Med. 352 (2005) 476–487.
[42] C. Castro, M. Gourley, Diagnostic testing and interpretation of tests for autoimmunity, J. Allergy Clin. Immunol. 125 (2010) S238–S247.
[43] L.B. Vong, Y. Nagasaki, Combination treatment of murine colon cancer with doxorubicin and redox nanoparticles, Mol. Pharm. 13 (2016) 449–455.
[44] I. Rahman, A. Kode, S.K. Biswas, Assay for quantitative determination of glutathione and glutathione disulfide levels using enzymatic recycling method, Nat. Prot. 1 (2006) 3159.
[45] S. Saha, L.S. New, H.K. Ho, W.K. Chui, E.C.Y. Chan, Direct toxicity effects of sulfoconjugated troglitazone on human hepatocytes, Toxicol. Lett. 195 (2010) 135–141.
[46] C. Maihofner, M.P. Charalambous, U. Bhambra, T. Lightfoot, G. Geisslinger, N.J. Gooderham, Expression of cyclooxygenase-2 parallels expression of interleukin-1beta, interleukin-6 and NF-kappaB in human colorectal cancer, Carcinogenesis 24 (2003) 665–671.
[47] H. Dalwadi, K. Krysan, N. Heuze-Vourc'h, M. Dohadwala, D. Elashoff, S. Sharma, et al., Cyclooxygenase-2-dependent activation of signal transducer and activator of transcription 3 by interleukin-6 in non-small cell lung cancer, Clin. Cancer Res. 11 (2005) 7674–7682.
[48] X.-H. Liu, A. Kirschenbaum, M. Lu, S. Yao, A. Klausner, C. Preston, et al., Prostaglandin E 2 stimulates prostatic intraepithelial neoplasia cell growth through activation of the interleukin-6/gp130/STAT-3 signaling pathway, Biochem. Biophys. Res. Commun. 290 (2002) 249–255.
[49] B.P. Ingalls, Mathematical Modeling in Systems Biology: An introduction, MIT Press.
[50] M. Frederich, B. Pirotte, M. Fillet, P. De Tullio, Metabolomics as a challenging approach for medicinal chemistry and personalized medicine, J. Med. Chem. 59 (2016) 8649–8666.
[51] J.P. Shockcor, Metabolic proles of cancer cells, Nat. Rev. Cancer 4 (2004) 551561.
[52] M. Rahman, M.R. Hasan, Cancer metabolism and drug resistance, Metabolites 5 (2015) 571–600.
[53] M.G. Vander, Heiden, Targeting cancer metabolism: a therapeutic window opens,

Nat. Rev. Drug Discov. 10 (2011) 671–684.
[54] Y. Asgari, Z. Zabihinpour, A. Salehzadeh-Yazdi, F. Schreiber, A. Masoudi-Nejad, Alterations in cancer cell metabolism: the Warburg effect and metabolic adaptation, Genomics 105 (2015) 275–281.
[55] S. Kim, S. Lee, Y.H. Maeng, W.Y. Chang, J.W. Hyun, S. Kim, Study of metabolic profiling changes in colorectal cancer tissues using 1D, Bull. Korean Chem. Soc. 34 (2017) 1467–1472.
[56] L. Wang, J. Chen, L. Chen, P. Deng, P. Xiang, M. Li, et al., 1H-NMR based metabonomic profiling of human esophageal cancer tissue, Mol. Cancer 12 (2013) 25.
[57] S. Bae, C.M. Ulrich, M.L. Neuhouser, O. Malysheva, L.B. Bailey, L. Xiao, et al., Plasma choline metabolites and colorectal cancer risk in the Women's Health Initiative Observational Study, Cancer Res. 74 (2014) 7442–7452.
[58] A. Guleria, A. Pratap, D. Dubey, A. Rawat, S. Chaurasia, E. Sukesh, et al., NMR based serum metabolomics reveals a distinctive signature in patients with Lupus Nephritis, Scientific Reports 6 (2016), http://dx.doi.org/10.1038/srep35309 Article number: 35309.
[59] M. Keenan, J.-T. Chi, Alternative fuels for cancer cells, Cancer J. 21 (2015) 49–55.
[60] G.K. Balendiran, R. Dabur, D. Fraser, The role of glutathione in cancer, Cell Biochem. Funct. 22 (2004) 343–352.
[61] L. Jin, G.N. Alesi, S. Kang, Glutaminolysis as a target for cancer therapy, Oncogene 35 (2016) 3619–3625.